Reducing fluctuations in species composition facilitates artificial selection of microbial community function

Li Xie* and Wenying Shou*

Abstract

Multi-species microbial communities often display functions - biochemical activities unattainable by member species alone, such as fighting pathogens. To improve community function, we can artificially select communities by growing "Newborn" communities over "maturation time" into "Adult" communities, and selecting highest-functioning Adults to "reproduce" by diluting each into multiple Newborns of the next cycle. Community selection has been attempted a few times on complex communities, often generating mixed results that are difficult to interpret. Here, we ask how costly community function may be improved via mutations and community selection. We simulate selection of two-species communities where Helpers digest Waste and generate Byproduct essential to Manufacturers; Manufacturers divert a fraction of their growth to make Product. Community function, the total Product in an "Adult", is sub-optimal even when both species have been pre-optimized as monocultures. If we dilute an Adult into Newborns by pipetting (a common experimental procedure), stochastic fluctuations in Newborn composition prevents community function from improving. Reducing fluctuations via cell sorting allows selection to work. Our conclusions hold regardless of whether H and M are commensal or mutualistic, or variations in model assumptions.

Introduction

Multi-species microbial communities often display important *functions*, defined here as biochemical activities not achievable by member species in isolation. For example, a six-species microbial community, but not any member species alone, cleared relapsing *Clostridium difficile* infections in mice [1]. As another example, cellulose-degrading communities often harbor non-cellulolytic aerobic bacteria that, by depleting oxygen, establish a proper anaerobic environment for cellulolytic bacteria [2].

Community functions arise from *interactions* where an individual alters the physiology of another individual. Thus, to improve community function, one could identify and modify interactions [3, 4]. In reality, this is no trivial task given that even two species can engage in complex interactions: each can release tens or more compounds, many of which may influence the partner species in diverse fashions [5, 6, 7, 8]. Then, from this myriad of interactions, we will need to identify those critical for community function, and modify them by altering species genotypes or the abiotic environment.

Alternatively, one could artificially select for microbial communities exhibiting high community function. In theory, artificial selection can be applied to any population of entities. An entity can be an individual (Figure S1A), a mono-species group of individuals (Figure S1B), or a multi-species community (Figure S1C) [9]. The boundary of a group or a community is artificially imposed (e.g. in microtiter wells or fluidic droplets). Here in artificial community selection, we allow low-density "Newborn communities" (Newborns) to "mature" over time T into "Adult communities" (Adults) when cells grow and mutate, and

*Author of correspondence

choose Adult communities expressing the highest community function to reproduce by splitting each into multiple Newborns to start the next cycle. Artificial selection of multi-species communities is predicted to be more challenging than artificial selection of mono-species groups or individuals (see Figure S1 for an explanation).

How effective is community selection? So far, community selection has been attempted only several times [10, 11, 12, 13]. In simulations, multi-species communities were selected based on how similar or dissimilar various chemical concentrations in the community abiotic environment are to arbitrarily-chosen target values [10]. Indeed, community selection produced the intended response, although the response quickly leveled off and was generated even without mutations. Thus in these simulations, community selection likely acted on preexisting variations in community species composition. In experiments, complex microbial communities were selected to improve their abilities to degrade a pollutant or alter plant physiology [11, 12, 14, 15]. For example, microbial communities could be selected to promote early or late flowering in plants, and communities associated with early-flowering versus late-flowering have distinct species makeups [15]. Strikingly in other studies, a community trait may fail to improve despite selection, and may improve even in control experiments random communities were selected to reproduce [11, 12].

Intriguing as these selection attempts might be, how they operated is often unknown. First, is the trait under selection a community function or simply a trait of one member species? If the latter, then community selection is not even needed. Second, does selection act solely on species make-ups or also on newly-arising genotypes? If selection acts mainly on species make-ups, which is likely the case for previous experiments [15], then without immigration of new species, community function will quickly level off [10]. If selection acts on genotypes, then community function can potentially continue to improve as new genotypes emerge. Third, does community selection run counter to natural selection? For example, during pollutant remediation, microbes may pay a fitness cost to release a pollutant-degrading enzyme. In this case, selecting high-degradation communities would favor high-degraders, while natural selection would favor low-degraders. Alternatively, microbes may exploit pollutant as a nutrient for growth. In this case, high-degraders are also fast growers, and are favored by both natural selection and community selection. In this case, community selection may not even be necessary.

In this article, we seek to understand how to effectively perform community selection so that we can improve a phenotype that is costly to the individual but beneficial to community function. Unlike mathematical models that, for example, focus on two genotypes (e.g. contributing or not contributing to community function), we seek a greater level of biological realism by simulating mechanisms of species interactions and incorporating experimentally-measured mutational processes. This allows our theoretical insights to guide future experiments.

Results

Species coexistence in a Helper-Manufacturer community

We consider a community that can convert waste (such as cellulose) to a useful product (such as a biofuel or an anti-cancer drug). Such communities have been engineered in the laboratory [16, 17, 18, 19]. In our Helper-Manufacturer community (Figure 1A), Helper H but not Manufacturer M can grow by digesting Waste. Waste is supplied in excess and thus its concentration change does not affect H growth rate. As H grows, it releases Byproduct B, which serves as the only carbon source for M. Thus, M depends on H (obligatory commensalism). H and M also compete for a shared Resource R (such as reduced nitrogen). M invests f_P fraction of its growth potential ($f_P g_M$) to make Product P, and uses the rest $(1 - f_P)g_M$ for its actual biomass growth. Community function $P(T)$ is defined as the total amount of Product P accumulated when a newly-assembled "Newborn" community matures into an "Adult" community over maturation time T (Figure 1B). Thus, community function incurs a fitness cost f_P to M. In Methods Section 7, we explain problems associated with two alternative definitions of community function.

To convert Waste to Product, H and M must coexist. Species coexistence is possible since H and M engage in obligatory commensalism [20]. Once a Newborn is formed, H immediately starts to grow on Waste and Resource, while M needs to wait for H's Byproduct. Once Byproduct has accumulated, if M can grow faster than H to "catch up", then H and M can stably coexist: different initial species ratios will converge to a positive steady state (Figure 1C, bottom). This requires f_P to be sufficiently small because otherwise, M will always grow slower than H (or even stop growing when $f_P = 1$) and go extinct (Figure 1C, top).

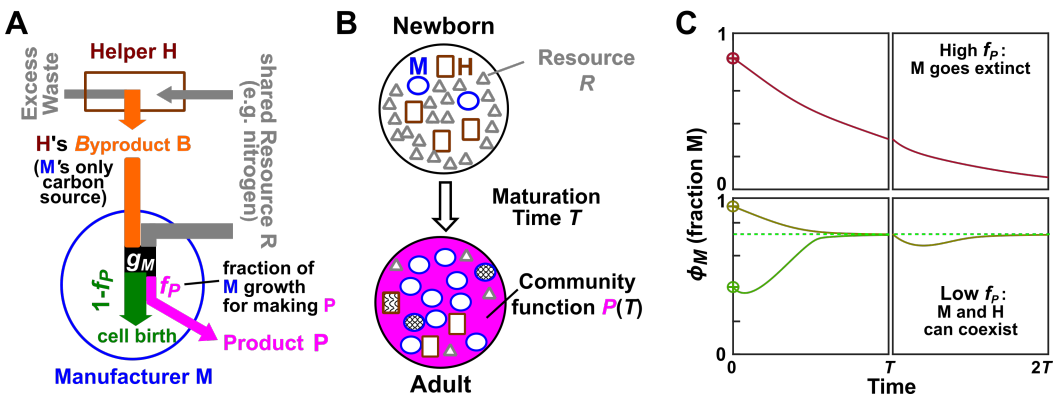

Figure 1: **Species coexistence in a Helper-Manufacturer community**. (**A**) A Helper-Manufacturer community, Helper H digests Waste to grow its biomass, and concomitantly releases Byproduct B. B is the sole carbon source for M. M invests a fraction f_P of its potential growth g_M to make Product P, while channeling the remaining $1 - f_P$ to its biomass growth. H and M compete for a shared Resource R. The release of Byproduct and Product is coupled to biomass growth. (**B**) Definition of community function. Different fill patterns represent mutant genotypes. (**C**) With our parameter choices (the last column of Table 1), H and M can stably coexist at low f_P (bottom; $f_P = 0.1$): different initial species ratios will converge to a stable equilibrium (dotted line). When f_P is high (top; $f_P = 0.8$), M goes extinct.

Simulating community selection

To simulate community selection experiments, we design our model (Methods Section 6) to be biologically realistic. Our parameter values (Table 1) are based on various experimental measurements on yeast and *E. coli* (details in Methods Section 2). As we will show, our conclusions are robust against variations in model assumptions.

Our model tracks individual cells. Cell biomass starts at 1, and once it grows to the division threshold of 2, the cell divides into two equal halves. Thus, our model captures continuous biomass increase (Figure S2) as well as discrete cell division events, similar to experimental observations of *E. coli* growth [21]. Biomass growth rate (g_H for H; $(1 - f_P)g_M$ for M) increases with concentration(s) of required nutrient(s) until maximal growth rate is achieved. For H, since Waste is in excess, we model growth rate as a function of Resource using the Monod Equation (Figure S3A). For M which requires both Resource and Byproduct, we adopt a dual-substrate model by Mankad and Bungay (Figure S3B) due to its experimental support [22] (Figure S4). Cell death occurs stochastically to individuals at a probability determined by death rate. Changes in quantities of metabolites (Resource R, Byproduct B, and Product P) are due to release and/or consumption.

f_P and growth parameters (maximal growth rates and affinities for metabolites) can mutate within the range of 0 and respective biological upper bounds (Table 1), as these phenotypes have been shown to evolve rapidly ([23, 24, 25, 26]). We choose ancestral growth parameters and their upper bounds so that

H and M can coexist for a sizable range of f_P (e.g. $f_P \leq 0.5$) during evolution. We hold H and M's death rates constant during evolution, because death rates are much smaller than growth rates and thus any changes are likely inconsequential. We also hold release and consumption parameters constant due to the stoichiometric constraints of biochemical reactions.

Experimentally-measured mutation rates vary from 10^{-8} to 10^{-3} phenotype-altering mutations (shorthanded as "mutations") per cell per generation depending on whether the phenotype is qualitative (e.g. survival under a stress) or quantitative (e.g. growth rate), and a variety of other factors (Methods Section 4). Mutation rate can be elevated by 100-fold in hyper-mutators with defective DNA repair machinery [27, 28, 29]. Here for each mutable phenotype, we assume a high but biologically feasible rate of 0.002 mutation per cell per generation, in part to speed up computation. 50% mutations create null mutants (f_P or growth phenotype =0), as per experiments on GFP, viruses, and yeast [30, 31, 32]. Effects of the other 50% mutations are exponentially distributed, enhancing or diminishing a phenotype by an average of 5% and 6.7% respectively, as per our re-analysis of published data sets [33] (Figure 2B). We further assume that the effects of sequential mutations are multiplicative (i.e. no epistasis). We will show that using a lower mutation rate, adopting a different of mutation effects, or incorporating epistasis does not alter our conclusions.

Variables of a selection regimen (Figure 2A) include the total number of communities under selection (n_{tot}), Newborn species biomass composition, the amount of Resource in Newborn, maturation time T, and how we reproduce an Adult. Large n_{tot} allows more variations to be selected, but experimental setup becomes more demanding. Here, we start with 100 Newborns which can be screened in 96-well plates. Species ratio will rapidly converge to a steady state value (Figure 1C, bottom). If Newborns have a large total biomass $N(0)$ or are allowed to grow to a large size, then all communities will share similar evolutionary dynamics of accumulating and being overtaken by non-producing Manufacturers [34, 35, 36], which impedes selection (similar to Figure S1B, top). At very small $N(0)$, a member species could get lost by chance, and a very large number of communities are required to sample those rare mutations that improve community function. Thus, we choose N_0, the target biomass of a Newborn community, to be 100 (e.g. 100 cells of biomass 1). The number of cell generations within a selection cycle should be sufficiently large to entertain new mutations, but sufficiently short to prevent non-producers from taking over. Thus, we supply each Newborn with Resource to support a maximal total biomass of 10^4, and set T such that the total biomass would grow from the initial ~100 to generally $\sim 6 \times 10^3$ even for the fastest-growing H and M. At the rate of 2×10^{-3} mutations per cell per generation, a community growing from $\sim 10^2$ to $\sim 6 \times 10^3$ ($\sim$ 6 generations) will on average sample ~20 new mutations per mutable phenotype. Within 6 generations, non-producers with a 20% fitness advantage over producers will rise from 2% to 6%, for example. Moreover, Resource will be in ~40% excess by the end of T, and this circumvents stationary phase. To reproduce an Adult, we do not allow mixing among communities to prevent non-producers from migrating to high-functioning communities. We reproduce the top-functioning Adult by randomly partitioning it into Newborns with $N(0) \sim$ target N_0. Experimentally, this can be achieved by calculating fold-dilution (dividing Adult turbidity by the target Newborn turbidity), and repeatedly pipetting 1/fold-dilution volume of Adult into fresh medium to form Newborns. Since total biomass generally increases by 10~60 fold during T depending on whether H and M are ancestral or evolved, each Adult can give rise to 10~60 Newborns. We then use the next top-functioning Adult until we generate $n_{tot} = 100$ Newborns for the next selection cycle.

Improving individual growth sometimes improves community function

When we select random Adults to reproduce, community function and average f_P rapidly decline to zero in all replicates (Figure S8B and C). This is expected since without community selection, natural selection favors fast-growing non-producers. Consistent with natural selection, maximal growth rates rapidly increase to their upper bounds, and nutrient affinities also improve (Figure S8A).

When we select top-functioning Adults to reproduce, $P(T)$ initially increases (Figure 3A). Average

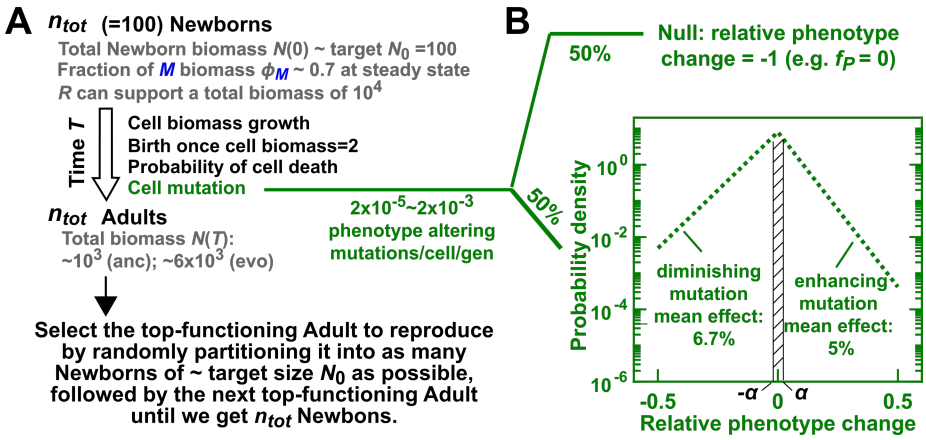

Figure 2: **Schematics of community selection.** (**A**) Summary of community selection simulation. (**B**) The distribution of mutation effects as inferred from [33] (see Figure S6 for full figure). For example in the case of f_P, 0.5 on the x-axis means $(f_{P,mut} - f_{P,anc})/f_{P,anc} = 0.5$. The probability of a mutation altering the relative phenotype by $\pm\alpha$ is the shaded area.

f_P ($\bar{f}_P$) does not decline, and remains at near the ancestral value. Concurrently, H and M's growth phenotypes (maximal growth rates and nutrient affinities) improve toward their respective upper bounds (Figure 3C). Improving individual growth does not always improve community function (Figure S9). For example, if H evolves to always grow faster than M, then H will out-compete M and community function will decline. However, we have chosen ancestral growth parameters and their biological upper bounds such that improving H and M's growth generally improves community function (Methods Section 3; Figures S10, S11, and S12). Thus, mutations that decrease growth parameters will be selected against by both natural selection and community selection. Fixing all growth parameters at their upper bounds greatly simplifies our analysis, as we demonstrate below.

f_P optimal for monoculture function may not be optimal for community function

It is unclear from Figure 3A how close the $P(T)$ plateau is to maximal $P^*(T)$. Given the nonlinear equations in our model (Methods Section 1), identifying global maximal is mathematically challenging.

Instead, after fixing all growth parameters to upper bounds and fixing total Newborn biomass to the target value ($N_0 = 100$), we can identify $f_P^* = 0.41$ (fraction of M growth diverted to making Product) and $\phi_M^*(0) = 0.54$ (fraction of M biomass in Newborn) corresponding to maximal community function $P^*(T) = 2735.5\tilde{r}_P$ (Methods, Section 3). For any $\phi_M(0)$, an intermediate f_P value maximizes community function (Figure 4A). This is not surprising: at zero f_P, no Product is made; at high f_P, H out-competes M. Importantly, the maximal $P^*(T)$ identified above cannot be further improved if we allow all growth and production parameters to mutate (Figure S14). Thus, $P^*(T)$ is locally maximal in the sense that small perturbations will always reduce $P(T)$.

Although community selection in Figure 3 yields H and M whose growth parameters are fixed at their upper bounds, $P(T)$ plateaus far below $P^*(T)$, and f_P remains far below f_P^*. To improve f_P, one might artificially select M for high production. Specifically, we may start with n_{tot} of 100 Newborn M groups, each inoculated with one M cell (to facilitate group selection, Figure S1B bottom panel). We supply each Newborn M group with the same amount of Resource as we supply Newborn H-M communities. For simplicity, we supply excess Byproduct to Newborn M groups since it is difficult to reproduce community Byproduct dynamics in M groups. Since here Newborn groups start with a single M individual, M-group selection can also be viewed as artificial selection of M individuals where the trait under selection is an

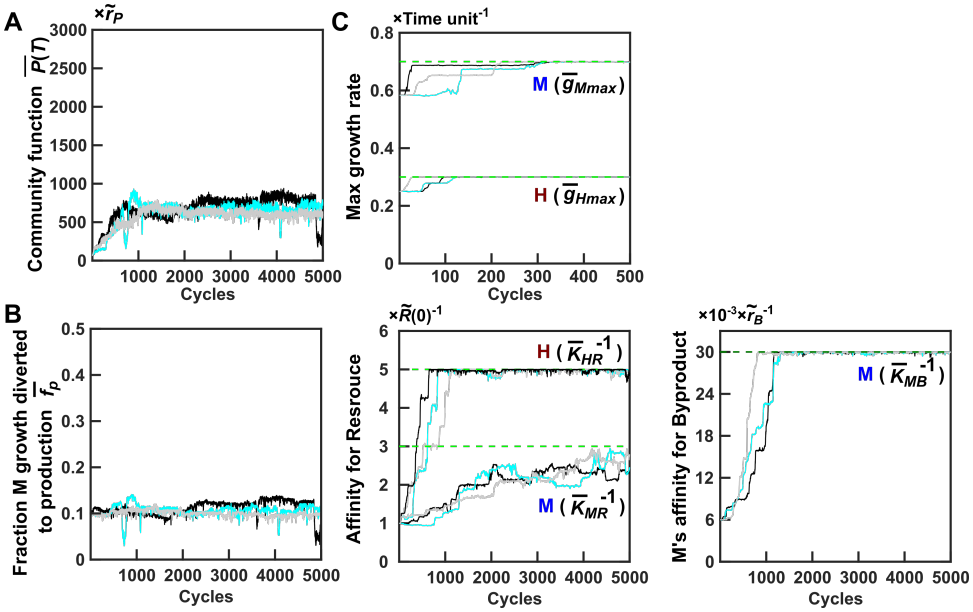

Figure 3: **Improved individual growth can promote community function.** Community function $P(T)$ increases upon community selection (**A**). Since f_P remains unchanged (**B**), this increase in $P(T)$ must be due to improved individual growth (**C**). Black, cyan, and gray curves show three independent simulations. Green dashed lines: upper bounds of the five growth parameters. Affinity for Resource ($1/K_{MR}$, $1/K_{HR}$) has the unit of $1/\widetilde{R}(0)$, where $\widetilde{R}(0)$ is the initial Resource in Newborn. Affinity for Byproduct ($1/K_{MB}$) has the unit of $1/\widetilde{r}_B$, where $\widetilde{r}_B$ is the amount of Byproduct released per H biomass produced. Product P has the unit of $\widetilde{r}_P$, the amount of Product released at the cost of one M biomass. $\overline{P}(T)$ is averaged across the two selected Adults. $\bar{g}_{Mmax}$, $\bar{g}_{Hmax}$, and $\overline{f}_P$ are obtained by averaging within each selected Adult and then averaging across the two selected Adults. $K_{SpeciesMetabolite}$ are averaged within each selected Adult, then averaged across the two selected Adults, and finally inverted to represent average affinity.

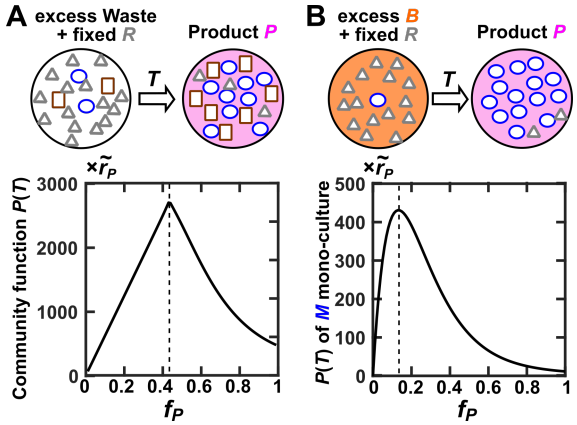

Figure 4: f_P **optimal for monoculture production is smaller than** f_P **optimal for community production. (A)** For a Newborn H-M community at a fixed total biomass $N(0) = 100$ and supplied with a fixed Resource and excess Waste, optimal $P(T)$ is achieved at an intermediate $f_P^* = 0.41$ (dashed line). Here the Newborn community has 54 M and 46 H cells of biomass 1, which corresponds to the species composition optimal for $P(T)$. **(B)** For a Newborn group starting with a single Manufacturer (biomass 1) supplied with the same amount of Resource and excess Byproduct, maximal group function is achieved at a lower $f_P = 0.13$ (dashed line). The growth parameters of M and H are all fixed at their upper bounds.

individual's ability to make Product over time T as the individual grows into a population. Regardless, our calculations show that f_P optimal for $P(T)$ in monocultures also occurs at an intermediate value (0.13; Figure 4B): at zero f_P , production is zero; at $f_P = 1$, M cannot grow and may even die, and thus $P(T)$ is low. Consistent with this calculation, when we select for high $P(T)$ in M groups, f_P gradually increases to 0.13 (Figure S15). However, f_P optimal for monoculture $P(T)$ is still much lower than f_P optimal for community $P(T)$ (Figure 4; see Methods Section 8 for an explanation). How can we perform community selection to improve f_P and $P(T)$ against natural selection's pressure of reducing them?

Community function fails to improve due to non-heritable variations

Starting with Newborns of mono-optimized H and M (all growth parameters at upper bounds and $f_P = 0.13$), we simulate artificial community selection (Figure 2; Methods Section 6). We only allow mutations to alter f_P as communities mature. Similar to Figure 3, we reproduce highest-functioning Adults by randomly partitioning them into Newborns with target total biomass N_0 (Figure 2C). Experimentally, this is equivalent to calculating the fold-dilution by dividing $N(T)$ (the turbidity of an Adult) by target N_0 (the target turbidity of a Newborn), and performing this dilution by pipetting an appropriate volume of the Adult community into fresh medium (Methods Section 6). In this selection regimen, total biomass $N(0)$ and fraction of M biomass $\phi_M(0)$ fluctuate stochastically in a Poissonian fashion (Methods Section 9). Similar to Figure 3, $\overline{f}_P$ and community function fail to increase and remain far below optimum (Figure 6A, B).

To investigate the reason for this lack of improvement, we examine correlation between $P(T)$ and Newborn composition in terms of average f_P ($\overline{f}_P(0)$), Newborn total biomass $N(0)$, and the fraction of M biomass in Newborn $\phi_M(0)$ (Figure 5). Here, $P(T)$ largely depends on Newborn composition because new genotypes do not have enough time to rise to high frequencies during the short T (6 generations) to impact $P(T)$. $P(T)$ should ideally depend on f_P whose variations are heritable. However during community selection, we observe little correlation between $P(T)$ and $\overline{f}_P(0)$ (Figure 5A). For example, the Adult displaying the highest function (left magenta dot) has a below-median $\overline{f}_P(0)$.

In contrast, $P(T)$ correlates strongly with $N(0)$ and $\phi_M(0)$ (Figure 5B-C). $N(0)$ and $\phi_M(0)$ can fluctuate stochastically during community reproduction. (Figure 5B-C; Methods 9). The reason for these strong

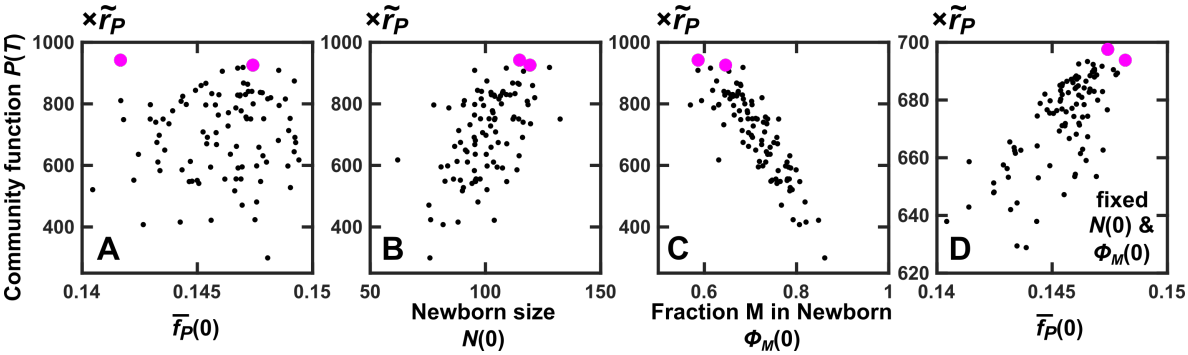

Figure 5: **Community function strongly correlates with Newborn total biomass and fraction of M biomass**. Correlations between $P(T)$ at Adulthood and Newborn compositions are plotted for 100 communities during one cycle of selection. Each dot represents one community. (**A**) $P(T)$ only weakly correlates with $\overline{f}_P(0)$ (f_P averaged over all M individuals in a Newborn). $\overline{f}_P(0)$ varies among Newborns due to stochastic sampling of M individuals with different f_P (Figure S16). If two Newborns are identical except $f_P = 0.14$ for one community and $f_P = 0.15$ for the other community, then $P(T)$ would differ by $\sim 7\%$. (**B-C**) In contrast, non-heritable Poissonian fluctuations in $N(0)$ and $\phi_M(0)$ during community reproduction cause large variations in $P(T)$. For example, at an average $N(0) = 100$, $N(0)$ can fluctuate in a Poissonian fashion by $\pm 3\sqrt{N(0)} = 30$ or 30%, which affects $P(T)$ by ~20%. Consequently, within these typical fluctuation ranges, $P(T)$ is impacted more by fluctuations in $N(0)$ and $\phi_M(0)$ than by variations in $\overline{f}_P(0)$, and selected communities (magenta dots) may not have the highest $\overline{f}_P(0)$. (**D**) When both $N(0)$ and $\phi_M(0)$ are fixed, $P(T)$ strongly correlates with $\overline{f}_P(0)$.

correlations becomes clear when we examine community dynamics. To minimize stationary phase, we have chosen maturation time T so that a typical community depletes the majority but not all of Resource. A Newborn begins with abundant Resource and no Byproduct, so H will grow first and release Byproduct. As Byproduct accumulates, M will start to grow. When a Newborn starts with a higher-than-average $N(0)$ (dotted lines in top panels of Figure S17), M will grow to a higher biomass, deplete Resource more thoroughly, and make more Product. Similarly, if a Newborn starts with a lower-than-average $\phi_M(0)$ (dotted lines in bottom panels of Figure S17), it will have a higher-than-average fraction of Helper. Consequently, M will endure a shorter growth lag, grow to a higher biomass, deplete Resource more thoroughly, and make more Product. Stochastic fluctuations in $N(0)$ and $\phi_M(0)$ generate relatively large non-heritable variations in $P(T)$ compared to $P(T)$ variations caused by mutations in f_P (Figure 5 legend). Consequently, communities with the highest average f_P may not get selected (Figure 5A).

Reducing non-heritable variations enables community function to improve

Reducing non-heritable variations should enable community selection to work. Indeed, if we fix both $N(0)$ and $\phi_M(0)$ (Methods, Section 6), then $P(T)$ becomes strongly correlated with $\overline{f}_P(0)$ (Figure 5D). Both $\overline{f}_P$ and $P(T)$ improve (Figure 6, G and H) to near the optimal. Experimentally, this can be achieved by flow-sorting into each Newborn a fixed biomass of H and M based on, for example, cell fluorescence intensity. $P(T)$ improvement is not seen if either $N(0)$ or $\phi_M(0)$ is non-fixed (Figure 6, C-F). $P(T)$ also improves (Figure S18) if we distribute fixed H and M cell numbers (instead of biomass) into each Newborn (Methods, Section 6), which can be realized experimentally by flow sorting individual cells.

Alternatively, we can reduce non-heritable variations in $P(T)$ by extending maturation time T so that an average community will deplete Resource by T. In this selection regimen, Newborns still experience Poissonian fluctuations in $N(0)$ and $\phi_M(0)$ during community reproduction. However, those "unlucky" communities with smaller-than-average $N(0)$ and/or larger-than-average $\phi_M(0)$ will have time to "catch

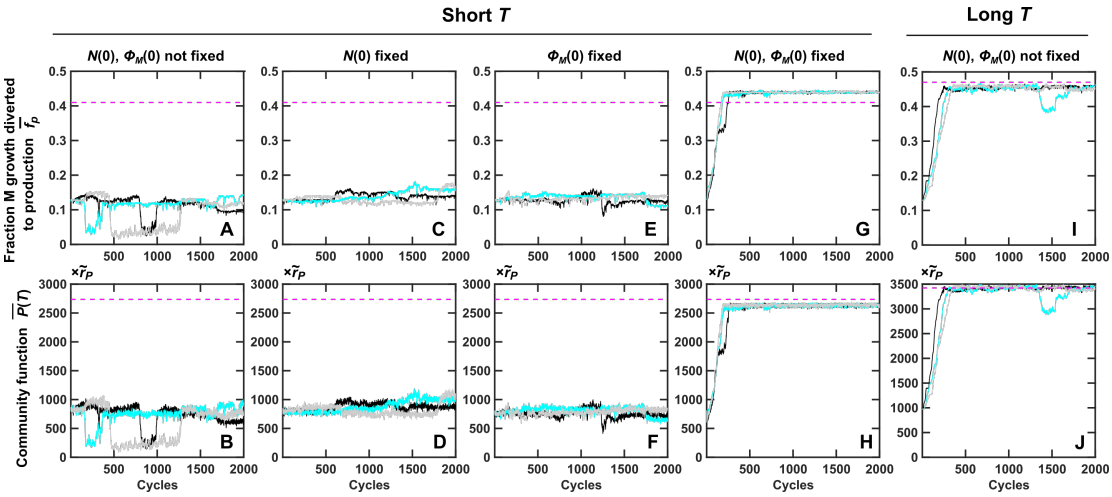

Figure 6: **Different selection regimens lead to qualitatively different community selection dynamics.** (**A-H**) Communities of mono-adapted H and M are selected for high $P(T)$ at short T (T=17, where on average 60% Resource is consumed by the end of T to avoid stationary phase). (**A, B**) $N(0)$ and $\phi_M(0)$ are allowed to fluctuate around target total biomass $N_0 = 100$ and $\phi_M(T)$ of the previous cycle (e.g. pipetting and diluting a portion of Adult into a Newborn). (**G, H**) $N(0)$ and $\phi_M(0)$ are fixed to $N_0 = 100$ and $\phi_M(T)$ of the previous cycle (e.g. sorting a fixed H biomass and M biomass into Newborns). This allows community function to improve. (**C-F**) Fixing either $N(0)$ or $\phi_M(0)$ does not significantly improve community selection. (**I-J**) Longer $T = 20$ is used. Community function improves under selection even without fixing $N(0)$ or $\phi_M(0)$. This is because Resource is nearly depleted by the end of T on average, and "unlucky" communities with lower $N(0)$ and/or higher $\phi_M(0)$ will have a chance to catch up as "lucky" communities wait in stationary phase. Magenta dashed lines: f_P^* optimal for $P(T)$ and maximal $P^*(T)$ when all five growth parameters are fixed at their upper bounds and $\phi_M(0)$ is at $\phi_M^*(0)$. Black, cyan and gray curves are three independent simulations. $\overline{P}(T)$ is averaged across the two selected Adults, and $\overline{f}_P$ is obtained by averaging within each selected Adult and then averaging across the two selected Adults.

up" as the "lucky" communities wait in stationary phase after exhausting Resource. Indeed, community function improves without having to fix $N(0)$ or $\phi_M(0)$ (Figure 6, **I-J**). In practice, these selection regimens will only be effective if variations in stationary phase duration introduce minimal non-heritable variations in community function.

In summary, seemingly innocuous experimental procedures such as pipetting can introduce a sufficiently large non-heritable variations in community function to stall selection. If we suppress these non-heritable variations, community function can rapidly improve. These conclusions hold when we use a different mutation rate (2×10^{-5} instead of 2×10^{-3} per cell per generation, Figure S19), a different distribution of mutation effects (an non-null mutation increases or decreases f_P by on average 2%, Figure S20), or incorporating epistasis (Figure S21, an non-null mutation is more likely to reduce f_P if the current f_P is high, or enhance f_P if the current f_P is low; Methods Section 5; Figure S7). We have also modified the H-M community to be mutualistic. Specifically, Byproduct is now inhibitory to H. Thus, H benefits M by providing Byproduct, and M benefits H by removing Byproduct, similar to the syntrophic community of *Desulfovibrio vulgaris* and *Methanococcus maripaludis* [37]. We observe similar evolutionary dynamics in this mutualistic H-M community (Figure S22).

Discussion

How might we improve functions of multi-species microbial communities via artificial selection? Currently, the most common approach is to enrich for the appropriate species combination [11, 12, 14, 15, 13]. For example, soil microbial communities that promote early or late flowering can be selected over ~10 cycles, and the two types of communities have different species compositions [15]. However, if we solely rely on species combinations to improve community function, then without a constant influx of new species, community function will likely level off quickly [10].

Here, we consider artificial selection of communities with defined member species, with selection acting on genotypes. The conventional wisdom may suggest "you get what you select for". But is this true? We have studied a Helper-Manufacturer community where community function is costly to Manufacturer. For community selection to be effective, we need to ensure that member species can stably coexist (Figure 2). Improving individual fitness can improve community function (Figures 3 and S10), although under different parameter choices, this is not true (Figure S9). Despite pre-optimizing member species in monocultures, community function may still be sub-optimal (Figure 4) due to the difficulty in recapitulating community dynamics in monocultures. Further improvements in community function can be achieved via artificial community selection, if performed properly.

Many aspects need to be taken into consideration when performing artificial community selection. Although suppressing non-heritable variations in a trait will always increase selection efficacy, here we show that for community selection, large non-heritable variations in community function can readily arise during routine experimental procedures such as pipetting. For example, if we choose maturation time T such that Resource is in excess to avoid stationary phase, then pipetting a volume of an Adult to seed a Newborn can already introduce non-heritable variations in community function (Figure 5B-C) sufficiently large to impede selection (Figure 6A-B). In contrast, if we fix both $N(0)$ and $\phi_M(0)$ (via cell sorting for example), then community function rapidly improves (Figure 6G-H). If we extend maturation time T so that Resource will on average be nearly depleted by the end of T, then community function also improves (Figure 6I-J), provided that variations in stationary phase duration will not generate large, non-heritable variations in community function. We observe similar phenomena when we vary model assumptions such as using a lower mutation rate (Figure S19), employing a different distribution of mutation effects (Figure S20), considering epistatsis (Figure S21), as well as in mutualistic H-M communities (Figure S22).

In the work of Ref. [11], authors tested two selection regimens with Newborn sizes differing by 100-fold. The authors hypothesized that smaller Newborns would have a high level of variation which should facilitate selection. However, the hypothesis was not corroborated by experiments, and as a possible explanation, the authors invoked the "butterfly effect" (the sensitivity of chaotic systems to initial conditions). Our results suggest that even for non-chaotic systems like the H-M community, selection could fail because fluctuations in species compositions in small Newborns compromise heredity.

A general ramification of our theory is that before launching a selection experiment, we should experimentally evaluate how much non-heritable variations in community function might arise under different selection regimens. One could inoculate replicate Newborns with as identical initial conditions as possible (e.g. via cell sorting). However, some levels of stochasticity, such as non-genetic phenotypic variations [38], stochasticity in cell birth and death, and errors in community function measurements, are inevitable. If community function variations among these replicate communities are significant compared to those among communities harboring different genotypes (i.e. noise is large compared to signal), community selection may be ineffective. On the other hand, if variations among replicate communities are small, then one can test whether less precise procedures such as cell culture pipetting could be used instead.

How does artificial selection of multi-species communities compare with artificial selection of mono-species groups? Group selection, and in a related sense, kin selection [39, 40, 41, 34, 42, 43, 44, 45, 46, 47, 48, 49, 50, 51, 52], have been extensively examined to explain, for example, the evolution of traits that lower individual fitness (e.g. sterile ants) but increase the success of a group. In both group selection and community selection, Newborn size must not be too large and maturation time must not be too

long, because otherwise, all entities will accumulate non-producers in a similar fashion, which interferes with selection [34, 53, 35] (Figure S1B). Community selection and group selection differ in two aspects. First, inter-species interactions in a community could drive species composition to a value sub-optimal for community function ([54]), and this problem does not exist for group selection especially when individuals in a group do not differentiate into interacting subgroups. Second, in group selection, when a Newborn group starts with a small number of individuals, a fraction of Newborn groups will show high similarity to the Newborn of the previous cycle (Figure S1B, bottom panel). This heredity facilitates group selection. In contrast, when a Newborn community starts with a small number of total individuals, large stochastic fluctuations in Newborn community composition can interfere with community selection (Figure 6). In the extreme case, a member species can even get lost by chance. Even if a fixed number of cells from each species are sorted into Newborns, heredity is much reduced in community selection compared to group selection. For example, if Newborn groups are initiated with a single cooperator and if the highest-functioning Adult group has accumulated 50% cheaters, then 50% Newborns of the next cycle will be initiated with a single cooperator. In contrast, if a Newborn community starts with a single cooperator from each of the two species and if the highest-functioning Adult has accumulated 50% cheaters in each species, then only 50%×50%= 25% Newborns of the next cycle will be initiated with pure cooperators.

When the total population size of a Newborn community is small, then each Newborn will inherit a small subset of genotypes from its parent Adult. If many communities are under selection, then in rare Newborns, beneficial genotypes from multiple species are simultaneously sampled. These Newborns harbor beneficial genotypes at high frequencies due to small Newborn size, and thus bear limited resemblance to Newborns of the previous cycle. In this case, reduction of heredity actually speeds up community selection, similar to sexual recombination: sexual recombination reduces heredity, but when population size is large, sexual recombination speeds up adaptation [55, 56, 57].

Microbes can coevolve with each other and with their host in nature [58, 59, 60]. This coevolution is mainly driven by natural selection. Might microbial community as a whole become a unit of selection in nature? Our work suggests that if selection for a costly microbial community function should occur in nature, then mechanisms for suppressing non-heritable variations in community function should be in place.

Methods

1 A mathematical model of the H-M community

The initial conditions of a Newborn community include initial H biomass $H(0)$, initial M biomass $M(0)$, and the initial amounts of Resource $\widetilde{R}(0)$, Byproduct ($B(0) = 0$), and Product ($P(0) = 0$). Starting from these initial conditions, the dynamics of H-< community comprising homogeneous H and M populations can be described by the following equations.

H, the biomass of H, changes as a function of growth and death,

$$\frac{dH}{dt} = g_H(\hat{R})H - \delta_H H \tag{1}$$

Grow rate g_H depends on the level of Resource $\hat{R}$ as described by the Monod growth model (Figure S3)

$$g_H(\hat{R}) = g_{Hmax}\frac{\hat{R}}{\hat{R} + \hat{K}_{HR}}$$

where $\hat{K}_{HR}$ is the $\hat{R}$ at which $g_{Hmax}/2$ is achieved.

M, the biomass of M, changes as a function of growth and death,

$$\frac{dM}{dt} = (1 - f_P)\, g_M(\hat{R},\, \hat{B})M - \delta_M M \tag{2}$$

Growth rate g_M depends on the levels of Resource and Byproduct ($\hat{R}$ and $\hat{B}$) according to the Mankad-Bungay model [22]:

$$g_M(\hat{R},\, \hat{B}) = g_{Mmax}\frac{\hat{R}_M\hat{B}_M}{\hat{R}_M + \hat{B}_M}\left(\frac{1}{\hat{R}_M + 1} + \frac{1}{\hat{B}_M + 1}\right)$$

where $\hat{R}_M = \hat{R}/\hat{K}_{MR}$ and $\hat{B}_M = \hat{B}/\hat{K}_{MB}$ (Figure S3). $1 - f_P$ fraction of M growth is channeled to biomass increase. f_P fraction of M growth is channeled to making Product:

$$\frac{d\hat{P}}{dt} = \tilde{r}_P f_P g_M(\hat{R},\, \hat{B})M \tag{3}$$

where $\tilde{r}_P$ is the amount of Product made at the cost of one M biomass.

Resource $\hat{R}$ is consumed proportionally to the growth of M and H; Byproduct $\hat{B}$ is released proportionally to H growth and consumed proportionally to M growth:

$$\frac{d\hat{R}}{dt} = -\hat{c}_{RM} g_M(\hat{R},\, \hat{B})M - \hat{c}_{RH} g_H(\hat{R})H \tag{4}$$

$$\frac{d\hat{B}}{dt} = \tilde{r}_B g_H(\hat{R})H - \hat{c}_{BM} g_M(\hat{R},\, \hat{B})M \tag{5}$$

Here, $\hat{c}_{RM}$ and $\hat{c}_{RH}$ are the amounts of $\hat{R}$ consumed per M and H biomass, respectively. $\hat{c}_{BM}$ is the amount of $\hat{B}$ consumed per M biomass. $\tilde{r}_B$ is the amount of $\hat{B}$ released per H biomass grown. Our model assumes that Byproduct or Product is generated proportionally to H or M biomass grown, which is reasonable given the stoichiometry of metabolic reactions and the experimental support [61]. The volume of a community V is set to be 1, and thus cell or metabolite quantities (which are considered here) are numerically identical to cell or metabolite concentrations.

In equations above, scaling factors are marked by "~", and will become 1 after scaling. Variables and parameters with hats will be scaled and lose their hats afterwards. Variables and parameters without hats will not be scaled. We scale Resource-related variable ($\hat{R}$) and parameters ($\hat{K}_{MR}$, $\hat{K}_{HR}$, $\hat{c}_{RM}$, and $\hat{c}_{RH}$) against $\tilde{R}(0)$ (Resource supplied to Newborn), Byproduct-related variable ($\hat{B}$) and parameters ($\hat{K}_{MB}$ and $\hat{c}_{BM}$) against $\tilde{r}_B$ (amount of Byproduct released per H biomass grown), and Product-related variable ($\hat{P}$) against $\tilde{r}_P$ (amount of Product made at the cost of one M biomass). For biologists who usually think of quantities with units, the purpose of scaling (and getting rid of units) is to reduce the number of parameters. For example, H biomass growth rate can be re-written as:

$$\begin{aligned} g_H(\hat{R}) &= g_{Hmax}\frac{\hat{R}}{\hat{R} + \hat{K}_{HR}} \\ &= g_{Hmax}\left(\frac{\hat{R}}{\tilde{R}(0)}\right)\Bigg/\left(\frac{\hat{R}}{\tilde{R}(0)} + \frac{\hat{K}_{HR}}{\tilde{R}(0)}\right) \\ &= g_{Hmax}\frac{R}{(R + K_{HR})} \\ &= g_H(R) \end{aligned}$$

where $R = \hat{R}/\tilde{R}(0)$ and $K_{HR} = \hat{K}_{HR}/\tilde{R}(0)$. Thus, the unscaled $g_H(\hat{R})$ and the scaled $g_H(R)$ share identical forms. After scaling, the value of $\tilde{R}(0)$ becomes irrelevant (1 with no unit). Similarly, since $\hat{R}_M = \frac{\hat{R}}{\tilde{R}(0)}\Big/\frac{\hat{K}_{MR}}{\tilde{R}(0)} = \frac{R}{K_{MR}} = R_M$ and $\hat{B}_M = \frac{\hat{B}}{\tilde{r}_B}\Big/\frac{\hat{K}_{MB}}{\tilde{r}_B} = \frac{B}{K_{MB}} = B_M$, $g_M(\hat{R},\, \hat{B}) = g_M(R,\, B)$.

Thus, scaled equations are

$$\frac{dH}{dt} = g_H(R)H - \delta_H H \tag{6}$$

$$\frac{dM}{dt} = (1 - f_P)\, g_M(R,\, B)M - \delta_M M \tag{7}$$

$$\begin{aligned} \frac{dP}{dt} &= \frac{d\hat{P}}{\widetilde{r}_P dt} \\ &= f_P g_M(\hat{R},\, \hat{B})M \\ &= f_P g_M(R,\, B)M \end{aligned} \tag{8}$$

$$\begin{aligned} \frac{dR}{dt} &= \frac{d\hat{R}/\widetilde{R}(0)}{dt} \\ &= -\frac{\hat{c}_{RM}}{\widetilde{R}(0)} g_M(\hat{R},\, \hat{B})M - \frac{\hat{c}_{RH}}{\widetilde{R}(0)} g_H(\hat{R})H \\ &= -c_{RM} g_M(R,\, B)M - c_{RH} g_H(R)H \end{aligned} \tag{9}$$

$$\begin{aligned} \frac{dB}{dt} &= \frac{d\hat{B}/\widetilde{r}_B}{dt} \\ &= g_H(\hat{R})H - \frac{\hat{c}_{BM}}{\widetilde{r}_B} g_M(\hat{R},\, \hat{B})M \\ &= g_H(R)H - c_{BM} g_M(R,\, B)M \end{aligned} \tag{10}$$

We have not scaled time here, although time can also be scaled by, for example, the community maturation time. Here, time has the unit of unit time (e.g. hr), and to avoid repetition, we often drop the time unit. After scaling, values of all parameters (including scaling factors) are in Table 1, and variables in our model and simulations are summarized in Table 2.

2 Parameter choices

With Waste in excess, H can grow on Resource. For ancestral H, we set $g_{Hmax} = 0.25$, $K_{HR} = 1$ (i.e. K_{HR} is one unit of $\widetilde{R}(0)$) and $c_{RH} = 10^{-4}$. This way, ancestral H can grow by about 10-fold by the end of $T = 17$. These parameters are biologically realistic: time unit can be arbitrarily chosen, and if we choose hour as the unit, then g_{Hmax} translates to a doubling time of 2.8 hrs. For a *lys- S. cerevisiae* strain with lysine as Resource, un-scaled Monod constant is $\hat{K} = 1$ μM, and consumption $\hat{c}$ is 2 fmole/cell (Ref. [62], Figure 2 Source Data 1; bioRxiv). Thus, if we choose 10 μL as volume and 2 μM as initial Resource concentration, then $\widetilde{R}(0) = 2 \times 10^4$ fmole. After scaling, $K = \hat{K}\hat{V}/\widetilde{R}(0) = 0.5$ and $c = \hat{c}/\widetilde{R}(0) = 10^{-4}$/cell.

To ensure the coexistence of H and M, M must grow faster than H for part of the maturation cycle. Thus, i) g_{Mmax} must exceed g_{Hmax} (Figure 1) since we have assumed M and H to have the same affinity for R (Table 1); ii) M's affinity for Byproduct ($1/K_{MB}$) must be sufficiently large; and iii) Byproduct consumed per Manufacturer c_{BM} must be sufficiently small so that growth of M can be supported by H. Thus for ancestral M, we choose $g_{Mmax} = 0.58$ (equivalent to a doubling time of 1.2 hrs). We set $\hat{c}_{BM} = \frac{1}{3}$ units of r_B (i.e. $c_{BM} = \frac{1}{3}$). This means that Byproduct released during one H biomass growth is sufficient to generate 3 M biomass, which is biologically achievable ([63, 64]). When we choose $\hat{K}_{MB} = \frac{5}{3} \times 10^2$ units of $\widetilde{r}_B$ (i.e. $K_{MB} = \frac{5}{3} \times 10^2$), H and M can coexist for a range of f_P (Figure 1). This value is realistic. For example, let B be hypoxanthine. A hypoxanthine-requiring *S. cerevisiae* strain evolved

	Definition	Ancestral	Evolved
$\widetilde{r}_B$	amount of released $\hat{B}$ per H biomass grown	scaling factor, 1	no change
$\widetilde{r}_P$	amount of released $\hat{P}$ at the cost of one M biomass	scaling factor, 1	no change
$\widetilde{R}(0)$	initial amount of Resource in Newborn	scaling factor, 1	
f_P	fraction of M growth diverted to producing P	0.03	0.13#
K_{MR}	fold of $\widetilde{R}(0)$ at which $g_{Mmax}/2$ is achieved in excess B	1	1/3*
K_{MB}	amount of $\hat{B}$ at which $g_{Mmax}/2$ is achieved in excess R, scaled against $\widetilde{r}_B$	$\frac{5}{3} \times 10^2$	$\frac{1}{3} \times 10^{2}$*
K_{HR}	fold of $\widetilde{R}(0)$ at which $g_{Hmax}/2$ is achieved	1	1/5*
g_{Mmax}	maximal biomass growth rate of M	0.58/unit time	0.7*
g_{Hmax}	maximal biomass growth rate of H	0.25/unit time	0.3*
δ_M	death rate of M	3.5×10^{-3}/unit time	no change
δ_H	death rate of H	1.5×10^{-3}/unit time	no change
c_{RM}	fraction of $\widetilde{R}(0)$ consumed per M biomass grown	10^{-4}	no change
c_{RH}	fraction of $\widetilde{R}(0)$ consumed per H biomass grown	10^{-4}	no change
c_{BM}	amount of $\hat{B}$ consumed per M biomass grown, scaled against $\widetilde{r}_B$	$\frac{1}{3}$	no change
P_{mut}	mutation probability per cell division for each mutable phenotype	$2 \times 10^{-5} \sim 2 \times 10^{-3}$	

Table 1: Parameters for ancestral and mono-adapted H and M. Parameters in the "Ancestral" column are used for Figure 3, while those in the "Evolved" column are used for all other figures. For maximal growth rates, * represents evolutionary upper bound. For $K_{SpeciesMetabolite}$, * represents evolutionary lower bound, which corresponds to evolutionary upper bound for Species's affinity for Metabolite ($1/K_{SpeciesMetabolite}$). # is from Figure 4B. In Methods Section 2, we explain our parameter choices (including why we hold some parameters constant during evolution).

Symbols	Definition
$M(t)$, $H(t)$	The biomass of M or H in a community at time t
$N(t) = M(t) + H(t)$	The total biomass in a community at time t
$\phi_M(t)$	The fraction of M biomass at time t
N_0	Pre-set target total biomass of Newborns during community reproduction
$I_M(t)$, $I_H(t)$	The integer number of M or H cells in a community at time t
$\varphi_M(t)$	The fraction of M individuals at time t
$L_M(t)$, $L_H(t)$	The biomass (length) of an individual M or H cell at time t, ranged between 1 and 2
$P(t)$	The amount of Product P in a community at time t, scaled by $\widetilde{r}_P$
$R(t)$	The amount of Resource R in a community at time t, scaled by $\widetilde{R}(0)$
$B(t)$	The amount of Byproduct B in a community at time t, scaled by $\widetilde{r}_B$
n_D	The fold dilution when reproducing an Adult community
n_{tot}	Total number of communities under selection
T	Community maturation time, corresponding to the duration of a selection cycle

Table 2: A summary of variables used in the simulation.

under hypoxanthine limitation could achieve a Monod constant for hypoxanthine at 0.1 μM (bioRxiv). If the volume of the community is 10 μL, then $K_{MB} = \frac{5}{3} \times 10^2$ corresponds to an absolute release rate $\widetilde{r}_B = 0.1\,\mu M \times 10\mu\text{L}/(\frac{5}{3} \times 10^2) = 6$ fmole per releaser biomass born. At 8 hour doubling time, this translates to 6 fmole/(1 cell×8 hr)≈ 0.75 fmole/cell/hr, within the ballpark of experimental observation (~0.3 fmole/cell/hr, bioRxiv). As a comparison, a lysine-overproducing yeast strain reaches a release rate of 0.8 fmole/cell/hr (bioRxiv) and a leucine-overproducing strain reaches a release rate of 4.2 fmole/cell/hr ([64]). Death rates δ_H and δ_M are chosen to be 0.5% of the upper bound of maximal growth rate, which is within the ballpark of experimental observations (e.g. the death rate of a *lys-* strain in lysine-limited chemostat is 0.4% of maximal growth rate, bioRxiv).

Since the biomass of various microbes share similar compositions of elements such as carbon or nitrogen [65], we assume that H and M consume the same amount of R per new cell ($c_{RH} = c_{RM}$). Since $c_{RH} = c_{RM} = 10^{-4}$ after scaling against $\widetilde{R}(0)$, the maximum yield is 10^4 total biomass.

Growth parameters (maximal growth rates g_{Mmax} and g_{Hmax} and affinities for nutrients $1/K_{MR}$, $1/K_{MB}$, and $1/K_{HR}$) and production parameter ($f_P \in [0, 1]$) are allowed to change during evolution, since these phenotypes have been observed to rapidly evolve within tens to hundreds of generations ([23, 24, 25, 26]). For example, several-fold improvement in nutrient affinity [24] and ~20% increase in maximal growth rate [26] have been observed in experimental evolution. Thus we allow affinities $1/K_{MR}$, $1/K_{HR}$, and $1/K_{MB}$ to increase by 3-fold, 5-fold, and 5-fold respectively, and allow g_{Hmax} and g_{Mmax} to increase by 20%. These bounds also ensure that evolved H and M can coexist for $f_p < 0.5$, and that Resource is on average not depleted by T to avoid cells entering stationary phase. Although maximal growth rate and nutrient affinity can sometimes show trade-off (e.g. Ref. [24]), for simplicity we assume here that they are independent of each other. We hold metabolite consumption (c_{RM}, c_{BM}, c_{RH}) constant because conversion of essential elements such as carbon and nitrogen into biomass is unlikely to evolve quickly and dramatically, especially when these elements are not in large excess ([65]). Similarly, we hold the scaling factors $\widetilde{r}_P$ and $\widetilde{r}_B$ constant, assuming that they do not change rapidly during evolution due to stoichiometric constraints of biochemical reactions. We hold death rates (δ_M, δ_H) constant because they are much smaller than growth rates in general and thus any changes are likely inconsequential.

3 Choosing growth parameters to simplify evolutionary modeling

Although improving individual growth (maximal growth rate and affinity for metabolites) does not always lead to improved community function (Figure S9), we have chosen ancestral growth parameters and their upper bounds so that improving individual growth improves community function. This way, we can assemble Newborn communities using mono-adapted H and M where all growth parameters are fixed at their respective biological upper bounds.

Fixing growth parameters of H and M to upper bounds also allows us to identify a locally maximal community function: For a Newborn with total biomass $N(0) = 100$, we can calculate $P(T)$ under various f_P and $\phi_M(0)$. Since both numbers range between 0 and 1, we calculate $P(T, f_P = 0.01 \times i, \phi_M(0) = 0.01 \times j)$ for integers i and j between 1 and 99. There is a single maximum for $P(T)$ when $i = 41$ and $j = 54$. In other words, when Newborn total biomass is fixed to 100, if M invests $f_P^* = 0.41$ of its growth to make Product and fraction of M biomass in Newborn$\phi_M^*(0) = 0.54$, maximal community function $P^*(T)$ is achieved (Figure 4A; magenta dashed line in Figure 6).

Let's first consider the case where $f_P^* = 0.41$. If we fix four of the five growth parameters to their upper bounds, then as the remaining growth parameter improves, both individual fitness and community function increase (magenta lines in Figure S10). Thus, if community function is already maximized, then deviations (reductions) from growth parameter upper bounds are disfavored by both community selection and natural selection, and hence growth parameters are naturally fixed.

Now let's consider the case where $f_P = 0.13$, which is optimal for M-monoculture function (grey dotted line in Figure 4B) and our starting point for community selection. Community function and individual fitness generally increase as growth parameters improve (black dashed lines in Figure S10). However,

individual fitness declines slightly when M's affinity for Resource ($1/K_{MR}$) improves.

Mathematically speaking, this is a consequence of the Mankad-Bungay model [22] (Figure S4B). Let $\mathring{S}_1 = S_1/K_1$ and $\mathring{S}_2 = S_2/K_2$. Then,

$$\begin{aligned}\frac{\partial g}{\partial K_1} &= \frac{\partial g}{\partial \mathring{S}_1}\frac{\partial \mathring{S}_1}{\partial K_1} = \frac{\partial\left[g_{max}\frac{\mathring{S}_1\mathring{S}_2}{\mathring{S}_1+\mathring{S}_2}\left(\frac{1}{1+\mathring{S}_1}+\frac{1}{1+\mathring{S}_2}\right)\right]}{\partial \mathring{S}_1}\frac{\partial \mathring{S}_1}{\partial K_1} \\ &= g_{max}\frac{\mathring{S}_1\mathring{S}_2}{(\mathring{S}_1+\mathring{S}_2)K_1}\left(\frac{\mathring{S}_1}{(1+\mathring{S}_1)^2}-\frac{\mathring{S}_2}{\mathring{S}_1+\mathring{S}_2}\left(\frac{1}{1+\mathring{S}_1}+\frac{1}{1+\mathring{S}_2}\right)\right)\end{aligned}$$

If $\mathring{S}_1 \ll 1 \ll \mathring{S}_2$ (corresponding to limiting S_1 and abundant S_2),

$$\frac{\mathring{S}_1}{(1+\mathring{S}_1)^2}-\frac{\mathring{S}_2}{\mathring{S}_1+\mathring{S}_2}\left(\frac{1}{1+\mathring{S}_1}+\frac{1}{1+\mathring{S}_2}\right) \approx \frac{\mathring{S}_1}{(1+\mathring{S}_1)^2}-\frac{1}{1+\mathring{S}_1} = -\frac{1}{(1+\mathring{S}_1)^2} \tag{11}$$

and thus $\partial g/\partial K_1 < 0$. This is the familiar case where growth rate increases as the Monod constant decreases (i.e. affinity increases). However, if $\mathring{S}_2 \ll 1 \ll \mathring{S}_1$

$$\frac{\mathring{S}_1}{(1+\mathring{S}_1)^2}-\frac{\mathring{S}_2}{\mathring{S}_1+\mathring{S}_2}\left(\frac{1}{1+\mathring{S}_1}+\frac{1}{1+\mathring{S}_2}\right) \approx \frac{1}{\mathring{S}_1}-\frac{\mathring{S}_2}{\mathring{S}_1}\frac{1}{1+\mathring{S}_2} = \frac{1}{\mathring{S}_1(1+\mathring{S}_2)} \tag{12}$$

and thus $\partial g/\partial K_1 > 0$. In this case, growth rate decreases as the Monod constant decreases (i.e. affinity increases). This is equivalent to decreased affinity for the abundant nutrient improving growth rate. Transporter competition for membrane space [66] could lead to this result, since reduced affinity for abundant nutrient may increase affinity for rare nutrient.

In the case of M, let S_1 represent R and let S_2 represent B. Thus, K_1 corresponds to K_{MR} and K_2 corresponds to K_{MB}. At the beginning of each cycle, R is abundant and B is limiting (Eq. 12). Thus M cells with lower affinity for R will grow faster than those with higher affinity (Figure S11). At the end of each cycle, the opposite is true (Figure S11). As f_P decreases, M has the capacity to grow faster and the first stage becomes more important. Thus at low f_P, M can gain higher overall fitness by lowering affinity for R (Figure S11A), which decreaes $P(T)$ very slightly (Figure S11B).

Regardless, decreased M affinity for Resource ($1/K_{MR}$) only leads to a very slight increase in M fitness and a very slight decrease in $P(T)$. Moreover, this only occurs at low f_P at the beginning of community selection, and thus may be neglected. Indeed, if we start all growth parameters at their upper bounds and $f_P = 0.13$, and perform community selection while allowing all parameters to vary (Figure S12), then $1/K_{MR}$ decreases somewhat, yet the dynamics of f_P is similar to when we only allow f_P to change (compare Figure S12D with Figure 6A). Indeed, allowing both f_P and $1/K_{MR}$ to evolve does not change our conclusions as shown in Figure S13.

4 Mutation rate and phenotype spectrum

Among mutations, a fraction will be phenotypically neutral in that they do not affect the phenotype of interest. For example, the vast majority of synonymous mutations are neutral [67]. Experimentally, the fraction of neutral mutations is difficult to determine. Consider organismal fitness as the phenotype of interest. Whether a mutation is neutral or not can vary as a function of effective population size, and selection condition. For example, at low population size due to genetic drift (i.e. changes in allele frequencies due to chance), a beneficial or deleterious mutation may not be selected for or selected against, and is thus neutral with respect to selection [68, 69]. Mutations in an antibiotic-degrading gene can be neutral under low antibiotic concentrations, but deleterious under high antibiotic concentrations [70]. When considering single mutations, a larger fraction of neutral mutations is equivalent to a lower rate of phenotype-altering mutations. Herein, our "mutation rate" refers to the rate of mutations that either enhance a phenotype

("enhancing mutations") or diminish a phenotype ("diminishing mutations"). Enhancing mutations of maximal growth rate (g_{Hmax} and g_{Mmax}) and of nutrient affinity ($1/K_{HR}$, $1/K_{MR}$, $1/K_{MB}$) enhance the fitness of an individual ("beneficial mutations"). In contrast, enhancing mutations in f_p diminish the fitness of an individual ("deleterious mutations").

Depending on the phenotype, the rate of phenotype-altering mutations is highly variable. Although mutations that cause qualitative phenotypic changes (e.g. drug resistance) occur at a rate of 10^{-8}~10^{-6} per genome per generation in bacteria and yeast [71, 72], mutations affecting quantitative traits such as growth rate occur much more frequently. For example in yeast, mutations that increase growth rate by $\geq 2\%$ occur at a rate of $\sim 10^{-4}$ per genome per generation (calculated from Figure 3 of Ref. [73]), and mutations that reduce growth rate occur at a rate of $10^{-4} \sim 10^{-3}$ per genome per generation [32, 29]. Moreover, mutation rate can be elevated by as much as 100-fold in hyper-mutators where DNA repair is dysfunctional [27, 28, 29]. Here for a mutable phenotype, we assume a high, but biologically feasible, rate of 2×10^{-3} phenotype-altering mutations per cell per generation to speed up computation. We have also tried 100-fold lower mutation rate. As expected, evolutionary dynamics slows down, but all of our conclusions still hold (Figure S19).

Among phenotype-altering mutations, tens of percent create null mutants, as illustrated by experimental studies on protein, viruses, and yeast [30, 31, 32]. Thus, we assume that 50% of phenotype-altering mutations are null (i.e. zero maximal growth rate, zero affinity for metabolite, or zero f_P). Among non-null mutations, the relative abundances of enhancing versus diminishing mutations are highly variable in different experiments. It can be impacted by effective population size. For example, with a large effective population size, the survival rate of beneficial mutations is 1000-fold lower due to clonal interference (competition between beneficial mutations) [74]. The relative abundance of enhancing versus diminishing mutations also strongly depends on the starting phenotype [30, 70, 68]. For example with ampicillin as a substrate, the TEM-1 β-lactamase acts as a "perfect" enzyme. Consequently, mutations were either neutral or diminishing, and few enhanced enzyme activity [70]. In contrast with a novel substrate such as cefotaxime, the enzyme had undetectable activity, and diminishing mutations were not detected while 2% of tested mutations were enhancing [70]. When we model H-M communities, we assume that the ancestral H and M have intermediate phenotypes that can be enhanced or diminished.

We base our distribution of mutation effects on experimental studies where a large number of enhancing and diminishing mutants have been quantified in an unbiased fashion. An example is a study from the Dunham lab where the fitness effects of thousands of *S. cerevisiae* mutations were quantified under various nutrient limitations [33]. Specifically for each nutrient limitation, the authors first measured $\triangle s_{WT} = (w_{WT} - \bar{w}_{WT})/\bar{w}_{WT} = w_{WT}/\bar{w}_{WT} - 1$, the deviation in relative fitness of thousands of bar-coded wild-type control strains from the wild-type mean fitness. Due to experimental noise, $\triangle s_{WT}$ is distributed with zero mean and non-zero variance. Then, the authors measured thousands of $\triangle s_{MT}$, each corresponding to the relative fitness change of a bar-coded mutant strain with respect to the mean of wild-type fitness (i.e. $\triangle s_{MT} = (w_{MT} - \bar{w}_{WT})/\bar{w}_{WT}$). From these two distributions, we derive $\mu_{\Delta s}$, the probability density function (PDF) of relative fitness change caused by mutations $\Delta s = \triangle s_{MT} - \triangle s_{WT}$ (see Figure 2B for interpreting PDF), in the following manner.

First, we calculate $\mu_m(\triangle s_{MT})$, discrete PDF of mutant strain relative fitness change, with bin width 0.04. In other words, $\mu_m(\triangle s_{MT})$ =counts in the bin of $[\triangle s_{MT} - 0.02, \triangle s_{MT} + 0.02]$ / total counts/0.04 where $\triangle s_{MT}$ ranges from -0.6 and 0.6 which is sufficient to cover the range of experimental outcome. The Poissonian uncertainty of μ_m is $\delta\mu_m(\triangle s_{MT}) = \sqrt{\text{counts per bin}}$/total counts/0.04. Repeating this process for wild-type collection, we obtain PDF of wild-type strain relative fitness $\mu_w(\triangle s_{WT})$. Next, from $\mu_w(\triangle s_{WT})$ and $\mu_m(\triangle s_{MT})$, we derive $\mu_{\Delta s}(\Delta s)$, the PDF of Δs with bin width 0.04:

$$\mu_{\Delta s}(\Delta s = i \times 0.04) = 0.04 \times \sum_{j=-\infty}^{+\infty} \mu_w(j \times 0.04)\mu_m((i+j) \times 0.04). \tag{13}$$

assuming that $\triangle s_{MT}$ and $\triangle s_{WT}$ are independent from each other. Here, i is an integer from -15 to 15. The uncertainty for $\mu_{\Delta s}$ is calculated by propagation of error. That is, if f is a function of x_i ($i = 1, 2, ...,$

n), then s_f, the error of f, is $s_f^2 = \sum \left(\frac{\partial f}{\partial x_i} s_{x_i}\right)^2$ where s_{x_i} is the error or uncertainty of x_i. Thus,

$$\delta\mu_{\Delta s}(i) = 0.04 \times \sqrt{\sum_j \left[(\delta\mu_w(j)\mu_m(i+j))^2 + (\mu_w(j)\delta\mu_m(i+j))^2\right]} \tag{14}$$

where $\mu_w(j)$ is short-hand notation for $\mu_w(\triangle s_{WT} = j \times 0.04)$ and so on. Our calculated $\mu_{\Delta s}(\Delta s)$ with error bar of $\delta\mu_{\Delta s}$ is shown in Figure S6.

Our reanalysis demonstrates that distributions of mutation fitness effects $\mu_{\Delta s}(\Delta s)$ are largely conserved regardless of nutrient conditions and mutation types (Figure S6B). In all cases, the relative fitness changes caused by beneficial (fitness-enhancing) and deleterious (fitness-diminishing) mutations can be approximated by separate exponential distributions with different means s_+ and s_-, respectively. After normalization to have a total probability of 1, we have:

$$\mu_{\Delta s}(\Delta s) = \begin{cases} \frac{1}{s_+ + s_-(1-\exp(-1/s_-))} \exp(-\Delta s/s_+) & \text{if } \Delta s \geq 0 \\ \frac{1}{s_+ + s_-(1-\exp(-1/s_-))} \exp(\Delta s/s_-) & \text{if } -1 < \Delta s < 0 \end{cases} \tag{15}$$

We fit the Dunham lab haploid data (since microbes are often haploid) to Eq. 15, using $\mu_{\Delta s}(i)/\delta\mu_{\Delta s}(i)$ as the weight for non-linear least squared regression (green lines in Figure S6B). We obtain $s_+ = 0.050 \pm 0.002$ and $s_- = 0.067 \pm 0.003$.

Interestingly, exponential distribution described the fitness effects of deleterious mutations in an RNA virus significantly well [30]. Based on extreme value theory, the fitness effects of beneficial mutations are predicted to follow an exponential distribution [75, 76], which has gained experimental support from bacterium and virus [77, 78, 79] (although see [80, 73] for counter examples). Evolutionary models based on exponential distributions of fitness effects have shown good agreements with experimental data [74, 81].

We have also tried smaller average mutational effects based on measurements of spontaneous or chemically-induced (instead of deletion) mutations. For example, the fitness effects of nonlethal deleterious mutations in *S. cerevisiae* are mostly 1%~5% [32], and the mean selection coefficient of beneficial mutations in *E. coli* was 1%~2% [77, 74]. Thus, as an alternative, we choose $s_+ = 0.02$; $s_- = -0.02$, and obtain similar conclusions (Figure S20).

5 Modeling epistasis on f_P

Epistasis, where the effect of a new mutation depends on prior mutations ("genetic background"), is known to affect evolutionary dynamics. Epistatic effects have been quantified in various ways. Experiments on viruses, bacteria, yeast, and proteins have demonstrated that for two mutations that are both deleterious or random, viable double mutants experience epistatic effects that are nearly symmetrically distributed around a value near zero [82, 83, 84, 85, 86]. In other words, a significant fraction of mutation pairs show no epistasis, and a small fraction show positive or negative epistasis (i.e. a double mutant displays a stronger or weaker phenotype than expected from additive effects of the two single mutants). Epistasis between two beneficial mutations can vary from being predominantly negative [83] to being symmetrically distributed around zero [84]. Furthermore, a beneficial mutation tends to confer a lower beneficial effect if the background already has high fitness ("diminishing returns") [87, 84, 88].

A mathematical model by Wiser et al. incorporates diminishing returns epistasis [81]. In this model, beneficial mutations of advantage s in the ancestral background are exponentially distributed with probability density $\alpha \exp(-\alpha s)$, where $1/\alpha > 0$ is the mean advantage. After a mutation with advantage s has occurred, the mean advantage of the next mutation would be reduced to $1/[\alpha(1+gs)]$, where $g > 0$ is the "diminishing returns parameter". Wiser et al. estimates $g \approx 6$. This model quantitatively explains the fitness dynamics of evolving *E. coli* populations.

Based on experimental and theoretical literature, we model epistasis on f_P in the following manner. Let the relative mutation effect on f_P be $\Delta f_P = (f_{P,mut} - f_P)/f_P \geq -1$. Then, $\mu(\Delta f_P,\ f_P)$, the probability density function of Δf_P at the current f_P value, is described by a form similar to Eq. 15:

$$\mu(\Delta f_P,\ f_P) = \begin{cases} \frac{1}{s_+(f_P)+s_-(f_P)(1-\exp(-1/s_-(f_P)))} \exp(-\Delta f_P/s_+(f_P)) & \text{if } \Delta f_P \geq 0 \\ \frac{1}{s_+(f_P)+s_-(f_P)(1-\exp(-1/s_-(f_P)))} \exp(\Delta f_P/s_-(f_P)) & \text{if } -1 < \Delta f_P < 0 \end{cases} \tag{16}$$

Here, $s_+(f_P)$ and $s_-(f_P)$ are respectively the mean Δf_P for enhancing and diminishing mutations at current f_P. $s_+(f_P) = s_{+init}/(1 + g \times (f_P/f_{P,init} - 1))$, where $f_{P,init}$ is the f_P of the initial background (e.g. 0.13 for mono-adapted Manufacturer), s_{+init} is the mean enhancing Δf_P occurring in the initial background, and $0 < g < 1$ is the epistatic factor. Similarly, $s_-(f_P) = s_{-init} \times (1 + g \times (f_P/f_{P,init} - 1))$ is the mean $|\Delta f_P|$ for diminishing mutations at current f_P. In the initial background since $f_P = f_{P,init}$, we have $s_+(f_P) = s_{+init}$ and $s_-(f_P) = s_{-init}$ where $s_{+init} = 0.050$ and $s_{-init} = 0.067$ (Figure S6). For subsequent mutations, PDF of Δf_P is modified by epistatic factor g according to Eq. 16. Consistent with the diminishing returns principle, if current $f_P > f_{P,init}$, then a new enhancing mutation becomes less likely and its mean effect also becomes smaller, while a new diminishing mutation becomes more likely and its mean effect also becomes bigger (ensured by $g > 0$; Figure S7 right panel). Similarly, if current $f_P < f_{P,init}$, then a new enhancing mutation becomes more likely and its mean effect also becomes bigger, while a diminishing mutation becomes less likely and its mean effect also becomes smaller (ensured by $0 < g < 1$; Figure S7 left panel). In summary, our model captures not only diminishing returns of enhancing mutations, but also our understanding of mutational effects on protein stability [68].

6 Simulation code of community selection cycle

In our simulation, cell mutation, cell death, and community reproduction are stochastic. All other processes (biomass growth, cell division, and changes in chemical concentrations) are deterministic.

The code starts with a total of $n_{tot} = 100$ Newborn communities with identical configuration:

- each community has 100 total cells of biomass 1. Thus, total biomass $N(0) = 100$.
- 40 cells are H. 60 cells are M with identical f_P. Thus, $M(0) = 60$ and $\phi_M(0) = 0.6$.

In the beginning, a random number is used to seed the random number generator for each Newborn community, and this number is saved so that the sequence of random numbers used below can be exactly repeated for subsequent data analysis. The initial amount of Resource is 1 unit of $\widetilde{R}(0)$, the initial Byproduct is $B(0) = 0$. and the initial Product $P(0) = 0$. The cycle time is divided into time steps of $\Delta\tau = 0.05$.

Below, we describe in detail what happens during each step of $\Delta\tau$. During an interval $[\tau,\ \tau + \Delta\tau]$, Resource $R(t)$ and Byproduct $B(t)$ between $[\tau,\ \tau + \Delta\tau]$ are calculated by solving the following equations between $[\tau, \tau + \Delta\tau]$ with the initial condition $R(\tau)$ and $B(\tau)$ using the ode23s solver in Matlab:

$$\frac{dR}{dt} = -c_{RM} g_M(R,\ B) M(\tau) - c_{RH} g_H(R) H(\tau) \tag{17}$$

$$\frac{dB}{dt} = g_H(R) H(\tau) - c_{BM} g_M(R,\ B) M(\tau) \tag{18}$$

where $M(\tau)$ and $H(\tau)$ are the biomass of M and H at time τ, respectively. The solutions from Eq. 17 and 18 are used in the integrals below.

We track the phenotypes of every H and M cell which are rod-shaped organisms of a fixed diameter. Let the biomass (length) of an H cell be $L_H(\tau)$. The continuous growth of L_H during τ and $\tau + \Delta\tau$ can be described as

$$\frac{dL_H}{dt} = g_H(R) L_H$$

thus $L_H(\tau + \Delta\tau)$ is

$$\ln \frac{L_H(\tau + \Delta\tau)}{L_H(\tau)} = \int_{\tau}^{\tau+\Delta\tau} g_H(R)dt$$

and

$$L_H(\tau + \Delta\tau) = L_H(\tau) \exp\left(\int_{\tau}^{\tau+\Delta\tau} g_H(R)dt\right). \tag{19}$$

Similarly, let the length of an M cell be $L_M(\tau)$. The continuous growth of M can be described as

$$\frac{dL_M}{dt} = (1 - f_P)g_M(R,\, B)L_M.$$

Thus during the interval $[\tau,\, \tau + \Delta\tau]$,

$$\ln \frac{L_M(\tau + \Delta\tau)}{L_M(\tau)} = \int_{\tau}^{\tau+\Delta\tau} (1 - f_P)g_M(R,\, B)dt$$

Thus for an M cell, its length $L_M(\tau + \Delta\tau)$ is

$$L_M(\tau + \Delta\tau) = L_M(\tau) \exp\left(\int_{\tau}^{\tau+\Delta\tau} (1 - f_P)g_M(R,\, B)dt\right) \tag{20}$$

From Eq. 7 and 8, within $\Delta\tau$,

$$\begin{aligned} \frac{dP}{dt} &= f_P g_M(R,\, B)M \\ &\sim \frac{f_P}{1 - f_P}\frac{dM}{dt} \end{aligned}$$

and we get

$$P(\tau + \Delta\tau) = P(\tau) + \frac{f_P}{1 - f_P}\left(M(\tau + \Delta\tau) - M(\tau)\right)$$

where $M(\tau + \Delta\tau) = \sum L_M(\tau + \Delta\tau)$ is the sum of the lengths of all M cells.

At the end of each $\Delta\tau$, each H and M cell has a probability of $\delta_H\Delta\tau$ and $\delta_M\Delta\tau$ to die, respectively. This is simulated by assigning a random number between [0, 1] for each cell and those receive a random number less than $\delta_H\Delta\tau$ or $\delta_M\Delta\tau$ get eliminated. For surviving cells, if a cell's length ≥ 2, this cell will divide into two cells with half the original length.

After division, each cell has a probability of $P_{mut} = 0.002$ to acquire a mutation that changes each of its mutable phenotype (Methods, Section 4). As an example, let's consider mutations in f_P. After mutation, f_P will be multiplied by $(1 + \Delta f_P)$, where Δf_P is determined as below.

First, a uniform random number u_1 between 0 and 1 is generated. If $u_1 \leq 0.5$, $\Delta f_P = -1$, which represents 50% chance of a null mutation ($f_P = 0$). If $0.5 < u_1 \leq 1$, Δf_P follows the distribution defined by Eq. 16 with $s_+(f_P) = 0.05$ for f_P-enhancing mutations and $s_-(f_P) = 0.067$ for f_P-diminishing mutations when epistasis is not considered (Methods, Section 4). In the simulation, Δf_P is generated via inverse transform sampling. Specifically, $C(\Delta f_P)$, the cumulative distribution function (CDF) of Δf_P , can be found by integrating Eq. 15 from -1 to Δf_P:

$$C(\Delta f_P) = \int_{-1}^{\Delta f_P} \mu_{\Delta s}(x)dx$$
$$= \begin{cases} \frac{s_-}{s_+ + s_-(1-e^{-1/s_-})} \left(\exp(\Delta f_P/s_-) - \exp(-1/s_-)\right) & \text{if } \Delta f_P \leq 0 \\ 1 - \frac{s_+}{s_+ + s_-(1-e^{-1/s_-})} \exp(-\Delta f_P/s_+) & \text{if } \Delta f_P \geq 0 \end{cases} \tag{21}$$

The two parts of Eq. 21 overlap at $C(\Delta f_P = 0) = s_-(1 - e^{-1/s_-})/\left[s_+ + s_-(1 - e^{-1/s_-})\right]$.

In order to generate Δf_P satisfying the distribution in Eq. 15, a uniform random number u_2 between 0 and 1 is generated and we set $C(\Delta f_P) = u_2$. Inverting Eq. 21 yields

$$\Delta f_P = \begin{cases} s_- \ln\left(u_2(s_+ + s_-(1 - e^{-1/s_-}))/s_- + e^{-1/s_-}\right) & u_2 \leq \frac{s_-(1-e^{-1/s_-})}{s_+ + s_-(1-e^{-1/s_-})} \\ -s_+ \ln\left((1 - u_2)(s_+ + s_-(1 - e^{-1/s_-}))/s_+\right) & u_2 > \frac{s_-(1-e^{-1/s_-})}{s_+ + s_-(1-e^{-1/s_-})} \end{cases} \tag{22}$$

When epistasis is considered, $s_+(f_P) = s_{+init}/(1 + g \times (f_P/f_{P,init} - 1))$ and $s_-(f_P) = s_{-init} \times (1 + g \times (f_P/f_{P,init} - 1))$ are used in Eq. 22 to calculated Δf_P for each cell with different current f_P (Methods Section 5).

If a mutation increases or decreases the phenotypic parameter beyond its bound, the phenotypic parameter is set to the bound value.

The above growth-death/birth-mutation cycle is repeated from time 0 to T. Note that since the size of each M and H cell can be larger than 1, the integer numbers of M and H cells, I_M and I_H, are generally smaller than biomass M and H , respectively. At the end of T, the communities are sorted according to $P(T)$.

For community reproduction, we save the current random number generator state to generate random numbers for partitioning the Adult. When we do not fix total biomass or total cell number or $\phi_M(0)$, we do the following. We select the Adult community with the highest function (or a randomly-chosen Adult community in control simulations). The fold by which this Adult will be diluted is $n_D = \lfloor (M(T) + H(T))/N_0 \rfloor$ where $N_0 = 100$ is the pre-set target for Newborn total biomass, and $\lfloor x \rfloor$ is the floor function that generates the largest integer that is smaller than x. $I_H + I_M$ random integers between 1 and n_D are uniformly generated so that each M and H cell is assigned a random integer between 1 and n_D. All cells assigned with the same random integer belong to the same Newborn. This generates n_D newborn communities. This partition regimen can be experimentally implemented by pipetting $1/n_D$ volume of an Adult community into a new well. If n_D is less than n_{tot} (the total number of communities under selection), all n_D newborn communities are kept. Then, we partition the Adult with the next highest function (or a random community in control simulations) to obtain an additional batch of n_D Newborns until we obtain n_{tot} Newborns. The next cycle then begins.

To "fix" Newborn total biomass $N(0)$ to the target total biomass N_0 (while allowing $\phi_M(0)$ to fluctuate), total biomass $N(0)$ is counted so that $N(0)$ comes closest to the target N_0 without exceeding it (otherwise, $P(T)$ may exceed the theoretical maximum). For example, suppose that a certain number of M and H cells have been sorted into a Newborn so that the total biomass is 98.6. If the next cell, either M or H, has a biomass of 1.3, this cell goes into the community so that the total biomass is $98.6 + 1.3 = 99.9$. However, if a cell of mass 1.6 happens to be picked, this cell doesn't go into this community so that this Newborn has a total biomass of 98.6 and the cell of mass 1.6 goes to the next Newborn. Thus, each Newborn may not have exactly the biomass of N_0, but rather between $N_0 - 2$ and N_0. Experimentally, total biomass can be determined from the optical density, or from the total fluorescence if cells are fluorescently labeled (bioRxiv). To fix Newborn total cell number (instead of total biomass), we perform simulations where the we sort a total of $\lfloor N_0/1.5 \rfloor$ cells into each Newborn, assuming that the average biomass of an M or H cell is 1.5. We obtain the same conclusion, as shown in Figure S18.

To fix $\phi_M(0)$ (while allowing $N(0)$ to fluctuate), we generate Newborn communities so that $\phi_M(0) = \phi_M(T)$ of the selected Adult community from the previous cycle. Again, because each M and H has a

biomass (or length) between 1 and 2, $\phi_M(0)$ of each Newborn community may not be exactly $\phi_M(T)$ of the selected Adult community. In the code, dilution fold n_D is calculated in the same fashion as mentioned above. $I_M(T)$ random integers between [1, n_D] are then generated for each M cell. All M cells assigned the same random integer belong to the same Newborn community. A total biomass of $M(0)(1-\phi_M(T))/\phi_M(T)$ of H cells should be sorted into this Newborn community. In the code, H cells are randomly dispensed into each Newborn community until the total biomass of H comes closest to $M(0)(1-\phi_M(T))/\phi_M(T)$ without exceeding it. Again, because each H cell has a biomass between 1 and 2, the total biomass of H might not be exactly $M(0)(1-\phi_M(T))/\phi_M(T)$ but between $M(0)(1-\phi_M(T))/\phi_M(T)-2$ and $M(0)(1-\phi_M(T))/\phi_M(T)$. We have also performed simulations where the ratio of M and H cell numbers in the Newborn community, $I_M(0)/I_H(0)$, is set to $I_M(T)/I_H(T)$ of the Adult community, and obtain the same conclusion (Figure S18 center panels).

To fix $N(0)$ to N_0 and $\phi_M(0)$ to $\phi_M(T)$ of the parent Adult, M cells are randomly picked from the Adult until the total biomass of M comes closest to $N_0\phi_M(T)$ without exceeding it. H cells are sorted similarly. Because each M and H cells has a length between 1 and 2, the biomass of M can vary between $N_0\phi_M(T)-2$ and $N_0\phi_M(T)$ and the biomass of H can vary between $N_0(1-\phi_M(T))-2$ and $N_0(1-\phi_M(T))$. Although such a partition scheme does not completely eliminate variations in species composition among Newborn communities, such variations are sufficiently small so that community selection can improve $\overline{f}_P(T)$. We have also performed simulations where the total number of cells is set to $\lfloor N_0/1.5 \rfloor$ with $\lfloor N_0\varphi_M(T)/1.5 \rfloor$ M cells and $\lfloor N_0(1-\varphi_M(T))/1.5 \rfloor$ H cells where $\varphi_M(T) = I_M(T)/(I_M(T)+I_H(T))$ is calculated from the numbers instead of biomass of M and H cells. We obtain the same conclusion (Figure S18, right panels).

7 Problems associated with alternative definitions of community function and alternative means of reproducing an Adult

We describe problems associated with two alternative definitions of community function. Let's consider a simpler case where groups of Manufacturers are selected for high P, and cell death is negligible. We have

$$\frac{dM}{dt} = (1-f_P)g_M M \tag{23}$$

$$\frac{dP}{dt} = f_P g_M M \tag{24}$$

where biomass growth rate g_M is a function of B and R. When M and H compete for Resource, g_M also depends implicitly on f_P because f_P affects M:H and therefore B and R.

Since from Eq. 23 and 24

$$\frac{dM}{(1-f_P)dt} = \frac{dP}{f_P dt}$$

we have

$$P(T) = \frac{f_P}{1-f_P}\left(M(T)-M(0)\right) \approx \frac{f_P}{1-f_P}M(T)$$

if $M(T) \gg M(0)$. This is true if T is long enough for cells to double at least three or four times.

If we define community function as $P(T)/M(T)$ (total Product normalized against M biomass in Adult community), $P(T)/M(T) \approx \frac{f_P}{1-f_P}$. Under this definition, higher $\frac{f_P}{1-f_P}$ or higher f_P always leads to higher community function, and higher f_P in turn leads to M extinction (Figure 1).

If the community function is instead defined as $P(T)/M(0)$, then

$$\frac{P(T)}{M(0)} \approx \frac{f_P}{1-f_P}\frac{M(T)}{M(0)} = \frac{f_P}{1-f_P}\exp\left((1-f_P)\int_T g_M dt\right) \tag{25}$$

From Eq. 25, at a fixed f_P, $\frac{P(T)}{M(0)}$ increases as $\int_T g_M dt$ increases. $\int_T g_M dt$ increases as $\phi_M(0)$ decreases, since the larger fraction of Helper, the faster the accumulation of Byproduct and the larger $\int_T g_M dt$

(Figure S17B). Thus, we end up selecting communities with small $\phi_M(0)$ (Figure S5). This means that Manufactures could get lost during community reproduction, and community selection then fails.

If Resource is unlimited, then it will be problematic to reproduce an Adult by diluting it by a fixed-fold to Newborns. This is because with unlimited Resource, there is no competition between H and M. According to Eq. 25, $P(T)$ increases linearly with $M(0)$. $P(T)$ also increases with $H(0)$, since higher $H(0)$ leads to higher Byproduct and consequently higher $\int_T g_M dt$ in the exponent. Thus each cycle, communities with larger $N(0)$ (instead of higher f_p) will get selected.

8 f_P^* is smaller for M group than for H-M community

For groups or communities with a certain $\int_T g_M dt$, we can calculate f_P optimal for community function from Eq. 25 by setting

$$\frac{dP(T)}{df_p} = M(0)\frac{d}{df_p}\left[\frac{f_P}{1-f_P}\exp\left((1-f_P)\int_T g_M dt\right)\right] = 0$$

We have

$$\frac{1}{(1-f_P)^2}\exp\left((1-f_P)\int_T g_M dt\right) - \frac{f_P}{1-f_P}\int_T g_M dt \exp\left((1-f_P)\int_T g_M dt\right) = 0$$

or

$$1/\int_T g_M dt = f_P(1-f_P).$$

If $\int_T g_M dt \gg 1$, f_P is very small, then the optimal f_P for $P(T)$ is

$$f_P^* \approx \left(\int_T g_M dt\right)^{-1} \tag{26}$$

M grows faster in monoculture than in community because B is supplied in excess in monoculture while in community, H-supplied Byproduct is initially limiting. Thus, $\int_T g_M dt$ is larger in monoculture than in community. According to Eq. 26, $f_P^* = 1/\int_T g_M dt$ is smaller for monoculture than for community.

9 Stochastic fluctuations during community reproduction

$N(0)$ fluctuates in a Poissonian fashion with a standard deviation of $\sqrt{\mathrm{E}[N(0)]}$, where "E" means the expected value.

$M(0)$ and $H(0)$ fluctuate independently with a standard deviation of $\sqrt{\mathrm{E}[M(0)]} = \sqrt{N_0\phi_M(T)}$ and $\sqrt{\mathrm{E}[H(0)]} = \sqrt{N_0(1-\phi_M(T))}$, respectively. Therefore, $M(0)/H(0)$ fluctuates with a variance of

$$\begin{aligned}\mathrm{Var}[M(0)/H(0)] &= \left(\frac{\mathrm{E}[M(0)]}{\mathrm{E}[H(0)]}\right)^2\left[\frac{\mathrm{Var}[M(0)]}{(\mathrm{E}[M(0)])^2} - 2\frac{\mathrm{Cov}[M(0),\,H(0)]}{\mathrm{E}[M(0)]\mathrm{E}[H(0)]} + \frac{\mathrm{Var}[H(0)]}{(\mathrm{E}[H(0)])^2}\right]\\ &= \left(\frac{\phi_M(T)}{(1-\phi_M(T))}\right)^2\left[\frac{1}{N_0\phi_M(T)} + \frac{1}{N_0(1-\phi_M(T))}\right]\end{aligned}$$

where "Cov" means covariance and "Var" means variance, and $\phi_M(T)$ is the fraction of M biomass in the Adult community from which Newborns are generated.

10 Mutualistic H-M community

In the mutualistic H-M community, Byproduct inhibits the growth of H. According to [89], the growth rate of *E. coli* decreases exponentially as the exogenously added acetate concentration increases. Thus, we only need to modify the growth of H by a factor of $\exp(-B/B_0)$ where B is the concentration of Byproduct and B_0 is the concentration of Byproduct at which H's growth rate is reduced by e^{-1}~0.37:

$$\frac{dH}{dt} = \exp\left(-\frac{B}{B_0}\right)\frac{g_{Hmax}R}{R+K_{HR}}H - \delta_H H$$

The larger B_0, the less inhibitory effect Byproduct has on H and when $B_0 \to +\infty$ Byproduct does not inhibit the growth of H. For simulations in Figure S22, $B_0 = 2K_{MB}$.

Acknowledgment

We thank the following for discussions: members of the Shou group, Lin Chao (UCSD), Maitreya Dunham (UW Seattle), Corina Tarnita (Princeton), and Harmit Malik (Fred Hutch). We thank Alex Yuan (UW Seattle), Chichun Chen (Indiana University Bloomington), Bill Hazelton, Samuel Hart, David Skelding, and Doug Jackson for feedback on the manuscript. This research was supported by the High Performance Computing Shared Resource of the Fred Hutch (P30 CA015704).

Supplementary Figures

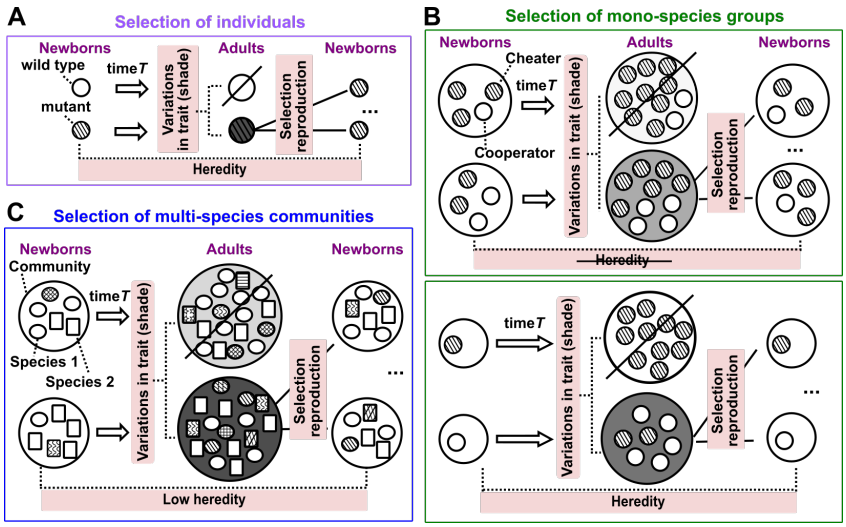

Figure S1: **Artificial selection can be more challenging for multi-species communities than for individuals or mono-species groups.** In artificial selection, the unit of selection can be an individual (**A**), a mono-species group (**B**), or a multi-species community (**C**). Unlike natural selection which selects for fastest-growing cells, artificial selection generally selects for traits that are costly to individuals. In each selection cycle, a population of "Newborn" entities grow for maturation time T to become "Adults". Adults expressing a higher level of the trait of interest (darker shade) are selected to reproduce. An individual reproduces by making copies of itself, while an Adult group or community can reproduce by randomly splitting into multiple Newborns. Successful artificial selection requires that i) entities display trait variations; ii) trait variations can be selected to result in differential entity survival and reproduction; and iii) entity trait is sufficiently heritable from one selection cycle to the next [90]. In all three types of selection, entity variations can be introduced by mutations and recombinations in individuals. Artificial selection also operates similarly. Below, we contrast the three types of selection. (**A**) Artificial selection of individuals has been successful [91, 92, 93], since a trait is largely heritable so long as mutation and recombination are sufficiently rare. (**B, C**) For group and community selection, if T is small to prevent new genotypes from rising to high frequency, then Adult trait is mostly determined by Newborn *composition* (the biomass of each genotype in each member species). Then, *variation* can be defined as the dissimilarity in Newborn composition within a selection cycle, and *heredity* as the similarity of Newborn composition from one cycle to the next. (**B**) Artificial selection of mono-species groups has been successful [43, 45, 94]. Consider "quorum sensing" group trait (e.g. producing toxin once an Adult group reaches a sufficiently high cell density) [95, 96]. Cooperators but not cheaters pay a fitness cost to generate toxin (shade). Artificial selection for groups with high total toxin favors cooperator-dominated groups, although within a group, cheaters grow faster than cooperators. At a large Newborn population size (**top**), relative fluctuations in genotype composition will be small. Thus, all Newborns will harbor similar fractions of cheaters, and inter-group variation will be small. During maturation, cheater frequency will increase, thereby diminishing heredity. In contrast, when Newborn groups are initiated at a small size such as one individual (**bottom**), a Newborn group will comprise either a cooperator or a cheater, thereby ensuring variation. Furthermore, even if cheaters were to arise during maturation, a fraction of Newborns of the next cycle will by chance inherit a cooperator, thereby ensuring some level of heredity. Thus, group selection can work when Newborn size is small. (**C**) Artificial selection of multi-species communities may be hindered by insufficient heredity. During maturation, the relative abundance of genotypes and species can rapidly change due to ecological interactions and evolution, which compromises heredity. During community reproduction, stochastic fluctuations in Newborn composition further reduce heredity.

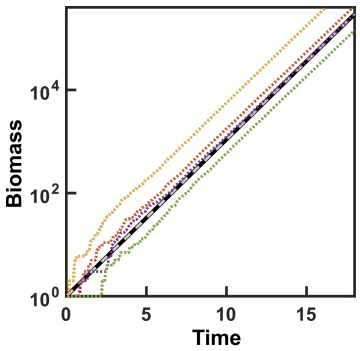

Figure S2: **A comparison of different growth models**. We model exponential biomass growth in excess metabolites. Thick black line: analytical solution with biomass growth rate (0.7/time unit). Grey dashed line: simulation assuming that biomass increases exponentially at 0.7/time unit and that cell division occurs upon reaching a biomass threshold, an assumption used in our model. Color dotted lines: simulations assuming that cell birth occurs at a probability equal to the birth rate multiplied with the length of simulation time step ($\Delta\tau = 0.05$ time unit). When a cell birth occurs, biomass increases discretely by 1, resulting in step-wise increase in color dotted lines at early time.

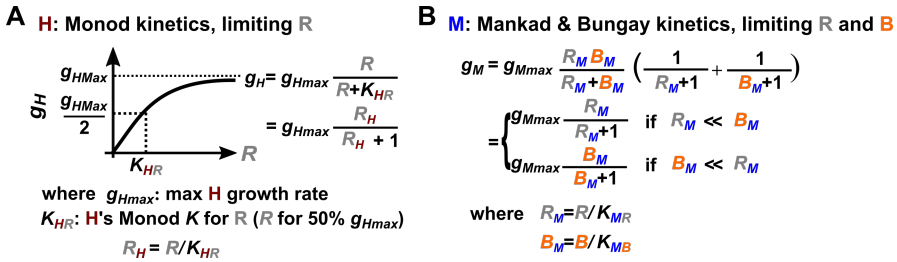

Figure S3: **Growth models of H and M.** (**A**) H growth follows Monod kinetics, reaching half maximal growth rate when $R = K_{HR}$. (**B**) M growth follows dual-substrate Mankad and Bungay kinetics. When Resource R is in great excess ($R_M \gg B_M$) or Byproduct B is in great excess ($B_M \gg R_M$), we recover mono-substrate Monod kinetics (**A**).

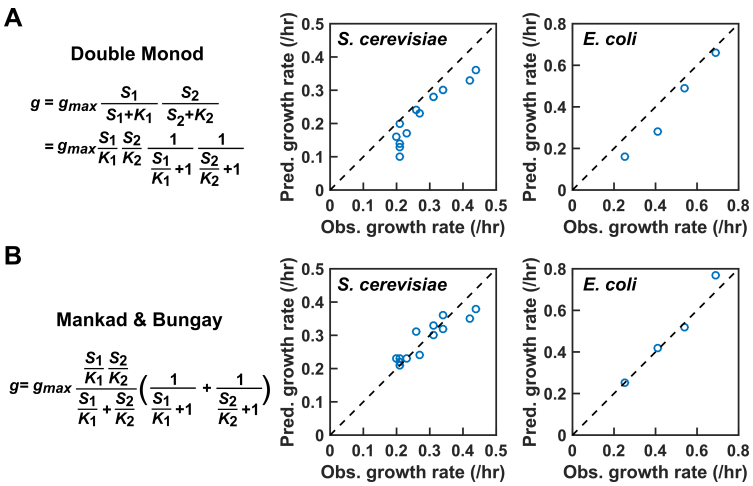

Figure S4: **A comparison of dual-substrate models.** Suppose that cell growth rate depends on each of the two substrates S_1 and S_2 in a Monod-like, saturable fashion. When S_2 is in excess, the S_1 at which half maximal growth rate is achieved is K_1. When S_1 is in excess, the S_2 at which half maximal growth rate is achieved is K_2. (**A**) In the "Double Monod" model, growth rate depends on the two limiting substrates in a multiplicative fashion. In the model proposed by Mankad and Bungay (**B**), growth rate takes a different form. In both models, when one substrate is in excess, growth rate depends on the other substrate in a Monod-fashion. However, when $\frac{S_1}{K_1} = \frac{S_2}{K_2} = 1$, the growth rate is predicted to be $g_{max}/2$ by Mankad & Bunday model, and $g_{max}/4$ by the Double Monod model. Mankad and Bungay model outperforms the Double Monod model in describing experimental data of *S. cerevisiae* and *E. coli* growing on low glucose and low nitrogen. The figures are plotted using data from Ref. [22].

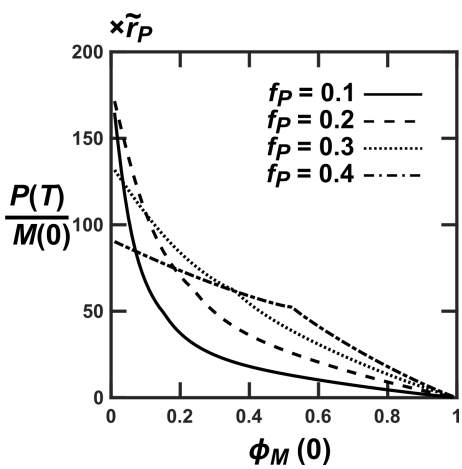

Figure S5: **Problems of defining community function as** $P(T)/M(0)$. Over the range of f_P where M and H can coexist, $P(T)/M(0)$ increases as $\phi_M(0)$ decreases. Thus, M can go extinct.

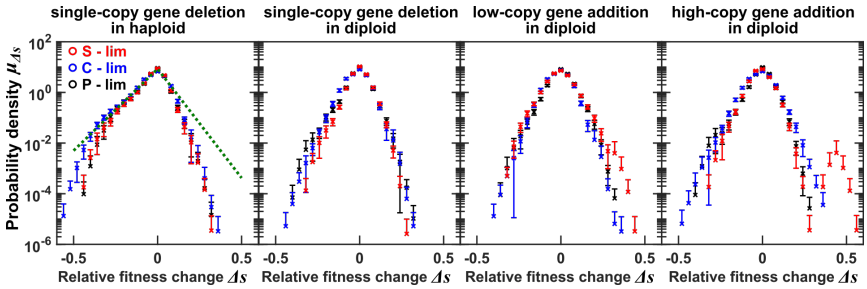

Figure S6: **Probability density functions of changes in relative fitness due to mutations ($\mu_{\Delta s}(\Delta s)$).** We derived $\mu_{\Delta s}(\Delta s)$ from the Dunham lab data [33] where bar-coded mutant strains were competed under sulfate-limitation (red), carbon-limitation (blue), or phosphate-limitation (black). Error bars represent uncertainty $\delta\mu_{\Delta s}$ (the lower error bar is omitted if the lower estimate is negative). In the leftmost panel, green lines show non-linear least squared fitting of data to Eq. 15 using all three sets of data. Note that data with larger uncertainty are given less weight, and thus deviate more from the fitting lines. For an exponentially-distributed probability density function $p(x) = \exp(-x/r)/r$ where x, $r > 0$, the average of x is r. When plotted on a semi-log scale, we get a straight line with slope $1/r$, and inverting this gets us the average effect r. From the green line on the right side, we obtain the average effect of enhancing mutations $s_+ = 0.050 \pm 0.002$, and from the green line on the left side, we obtain the average effect of diminishing mutations $s_- = 0.067 \pm 0.003$.

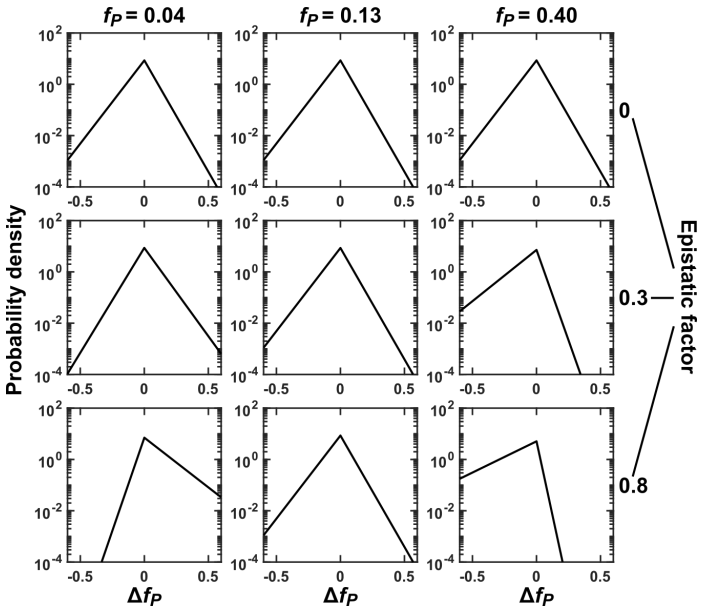

Figure S7: **Mutation effects under epistasis.** Distribution of mutation effects at different current f_P values are plotted. (Top) When there is no epistasis, distribution of mutational effects on f_P ($\triangle f_P$) are identical regardless of current f_P. (Middle and Bottom) With epistasis (see Methods Section 5 for definition of epistasis factor), mutational effects on f_P depend on the current value of f_P. If current f_P is low (left), enhancing mutations are more likely to occur (the area to the right of $\triangle f_P = 0$ becomes bigger) and their mean mutational effect becomes larger (mean=1/slope becomes larger due to smaller slope), while diminishing mutations are less likely to occur and their mean mutational effect is smaller. If current f_P is high (right), the opposite is true.

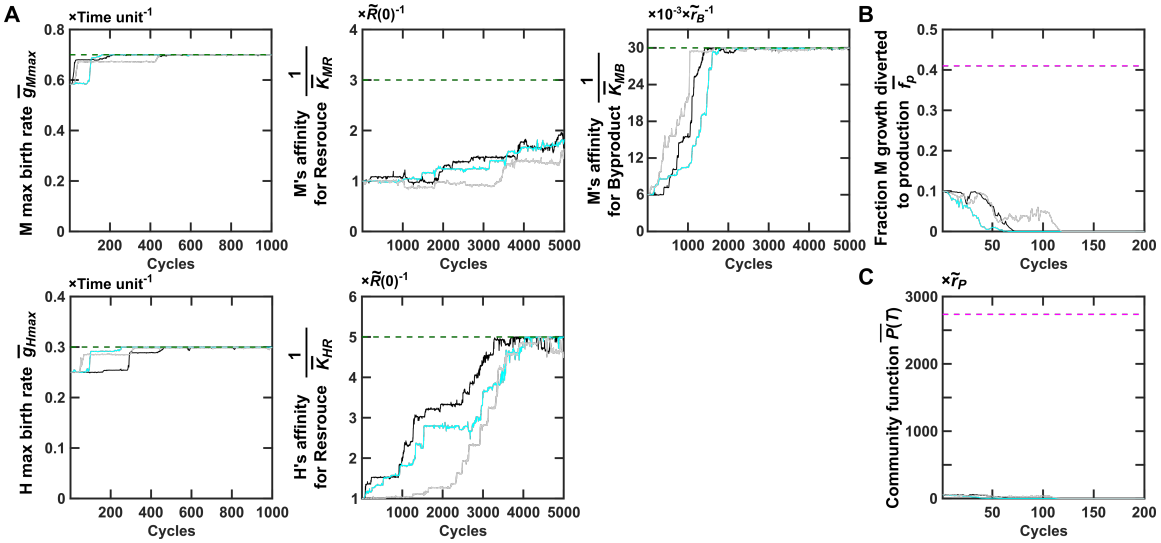

Figure S8: **Community function declines to zero in the absence of community selection**. Without community selection, natural selection favors fast growers with improved maximal growth rates and improved affinities for nutrients (**A**), and zero f_P (**B**). Consequently, $P(T)$ decrease to zero (**C**). Maximal growth rates of H and M (g_{Hmax} and g_{Mmax}), H's affinity for Resource $1/K_{HR}$, and M's affinity for Byproduct $1/K_{MB}$ rapidly improve to their respective upper bounds, while M's affinity for Resource $1/K_{MR}$ improves more slowly. This is consistent with M's growth being more limited by Byproduct. $\overline{P}(T)$ is averaged across the two randomly selected Adult communities. $\overline{g}_{Mmax}$, $\overline{g}_{Hmax}$, and $\overline{f}_P$ are obtained by averaging within each randomly-selected Adult community and then averaging across the two randomly-selected Adult communities. $K_{SpeciesMetabolite}$ are averaged within each randomly-selected Adult community, then across the two randomly-selected Adults, and finally inverted to represent average affinity. Green dashed lines: upper bounds of phenotypes; Magenta dashed lines: f_P optimal for community function and maximal $P(T)$ when all five growth parameters are fixed at their upper bounds and $\phi_M(0)$ is also optimal for $P(T)$. Note different x axis scales. Black, cyan, and gray curves show three independent simulations.

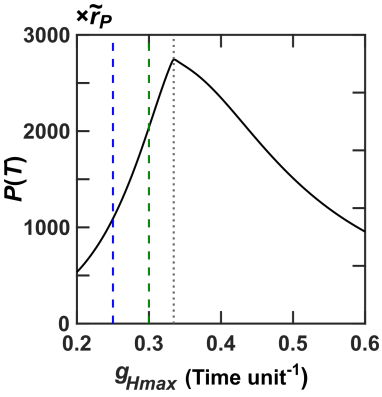

Figure S9: **Improving maximal growth rate of Helper g_{Hmax} does not necessarily improve community function**. We have chosen the ancestral (blue dashed line) and the biological upper bound (green dashed line) of g_{Hmax} such that improving g_{Hmax} improves community function. Suppose we have chosen ancestral g_{Hmax} at the grey dotted line, then higher g_{Hmax} would lower community function. The black solid curve is obtained by numerically integrating Eqs. 6-10 at different g_{Hmax} values where f_P is set to 0.4 and all growth parameters except for g_{Hmax} are set to their respective upper bounds. $N(0)$ is 100, and $\phi_M(0)$ is 0.7 (close to steady-state value).

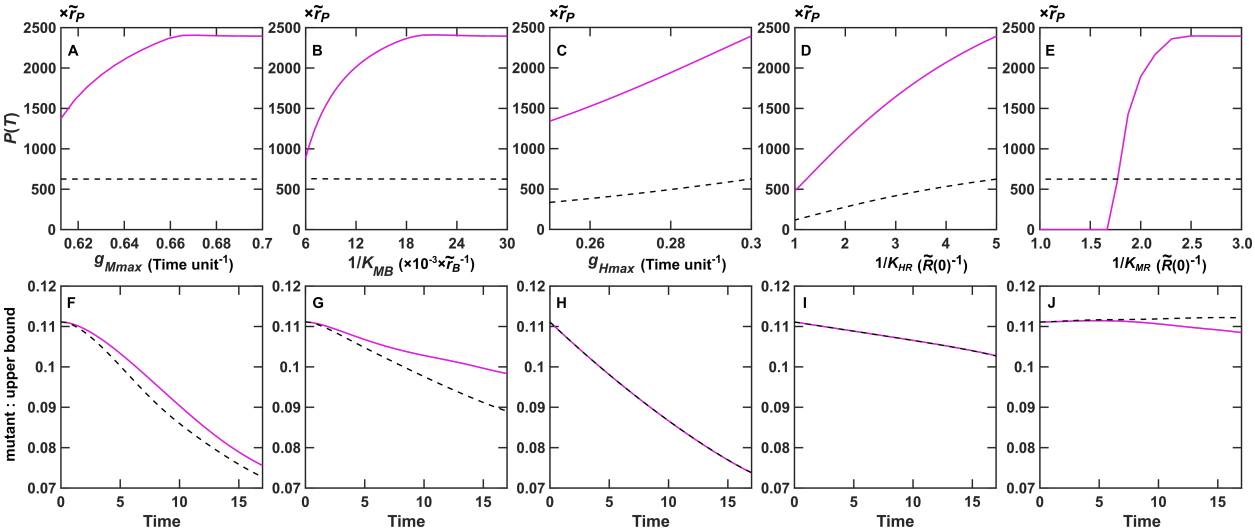

Figure S10: **Improving maximal growth rates and nutrient affinities generally, but do not always, improve individual fitness and community function.** In all figures, solid and dashed lines respectively represent dynamics when $f_P^* = 0.41$ (optimal for community function if all growth parameters are fixed at their upper bounds and $\phi_M(0) = 0.54$; Figure 4A) and $f_P = 0.13$ (optimal for M monoculture production when Byproduct is in excess; Figure 4B). (A-D) Community function increases as g_{Mmax}, $1/K_{MB}$, g_{Hmax} or $1/K_{HR}$ increases when other growth parameters are fixed at their upper bounds. For example, In (A), all growth parameters except for g_{Mmax} are at their upper bounds, and for each combination of g_{Mmax} and f_P, the steady-state $\phi_{M,SS}$ is calculated using equations in Methods Section 1. This steady-state $\phi_{M,SS}$ is then used to calculate $P(T)$. (F-I) respectively show that mutant individuals with g_{Mmax}, $1/K_{MB}$, g_{Hmax} or $1/K_{HR}$ 10% lower than the upper bound have lower fitness. For example in (F), a Newborn community has 70 M and 30 H. 90% of M have upper bound $g_{Mmax} = 0.7$ ("upper bound"). 10% of M have $g_{Mmax} = 0.63$, 10% less than the upper bound ("mutant"). Other growth parameters are all at upper bounds. The ratio between mutant and upper bound drops over maturation time, indicating that M cells with mutant (lower) maximal growth rate have lower fitness. (E, J) When $f_P = 0.13$ (black dashed line) but not when $f_P = 0.41$ (magenta line), increasing M's affinity for Resource ($1/K_{MR}$) slightly decreases individual fitness.

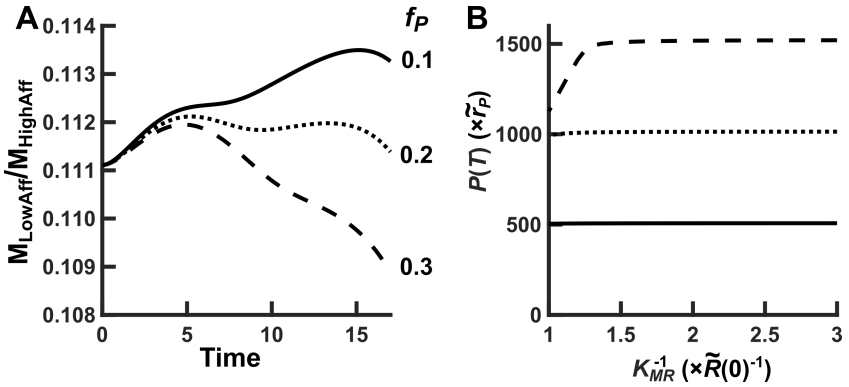

Figure S11: **At low f_P, higher $1/K_{MR}$ can lead to reduced M growth rate. (A)** The ratio between M_{LowAff} with low affinity for R ($K_{MR}^{-1} = 2.5\widetilde{R}(0)^{-1}$) and $M_{HighAff}$ with high affinity for R ($K_{MR}^{-1} = 3\widetilde{R}(0)^{-1}$) when their f_P is equal to 0.1 (solid line), 0.2 (dotted line) and 0.3 (dashed line) are plotted over one maturation cycle. **(B)** $P(T)$ improves over increasing affinity K_{MR}^{-1} when f_P is 0.1 (solid line), 0.2 (dotted line) and 0.3 (dashed line). The dependence of $P(T)$ on K_{MR}^{-1} is rather weak for low f_P. For example, when K_{MR}^{-1} increases from 1 to 3, $P(T)$ increases only by 2% and 0.6% for $f_P = 0.2$ and $f_P = 0.1$, respectively.

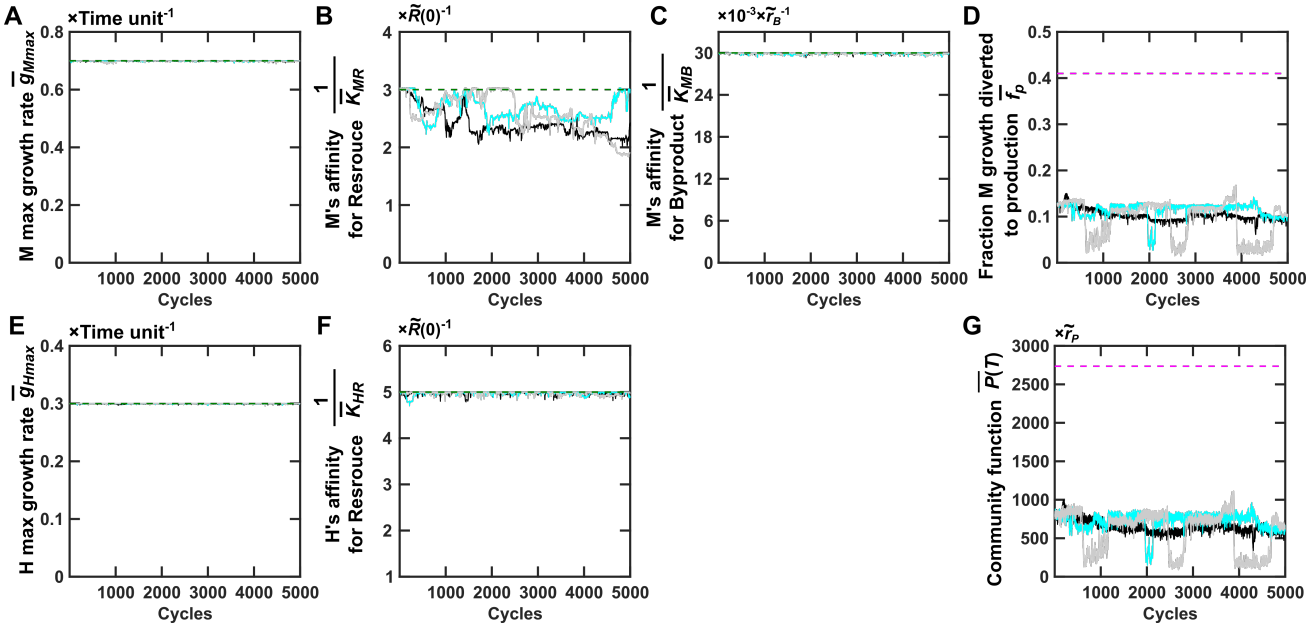

Figure S12: **Selection dynamics of communities of mono-adapted H and M when allowing all parameters to vary**. We start all growth parameters at their upper bounds and $f_P = 0.13$ (Figure 4B), and perform community selection while allowing all growth parameters and f_P to vary. $\bar{g}_{Mmax}$, $\bar{g}_{Hmax}$, $1/\bar{K}_{MB}$ and $1/\bar{K}_{HR}$ remain mostly constant during community selection because mutants with lower-than-maximal values are weeded out by natural selection as well as community selection. However, $1/\bar{K}_{MR}$ decreases slightly because at low $f_P = 0.13$, M with a lower affinity for R (lower $1/K_{MR}$) slightly improves individual fitness while slightly decreasing community function (Figure S11). $\bar{g}_{Mmax}$, $\bar{g}_{Hmax}$, and $\overline{f}_P$ are obtained by averaging within each selected Adult community and then averaging across the two selected Adults. $K_{SpeciesMetabolite}$ are similarly averaged, and then inverted to represent average affinity. $\overline{P}(T)$ are averaged across the two selected Adults. Black, cyan and gray curves are three independent simulations. Green dashed lines indicate upper bounds for growth parameters. Magenta dashed lines: f_P optimal for community function and optimal $P(T)$ when all five growth parameters are fixed at their upper bounds and $\phi_M(0)$ is also optimal for $P(T)$.

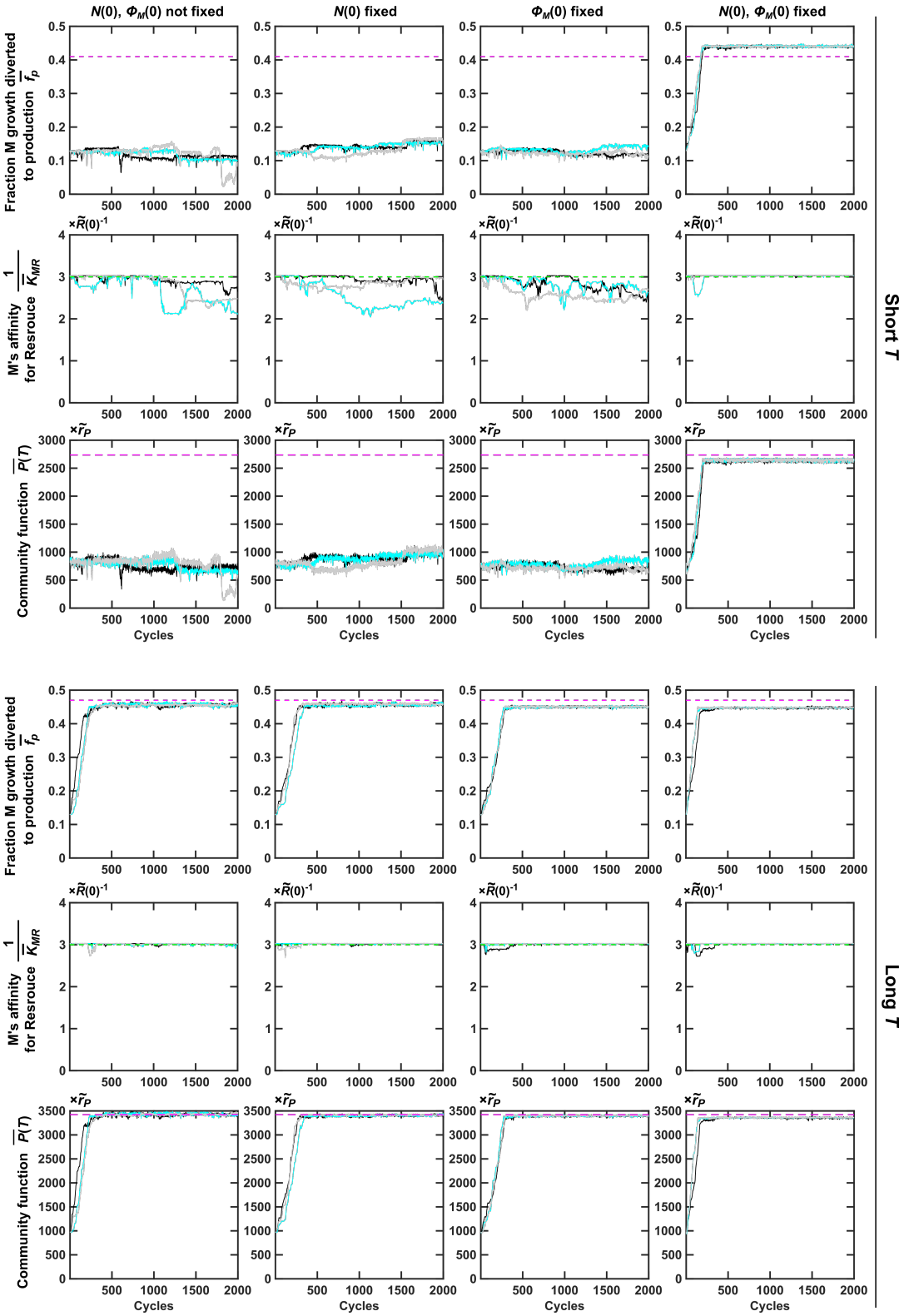

Figure S13: **Evolution dynamics of selected Adult communities when both f_P and K_{MR} are allowed to mutate.** Green dashed lines indicate upper bounds for growth parameters. Magenta dashed lines: f_P optimal for community function and optimal $P(T)$ when all five growth parameters are fixed at their upper bounds and $\phi_M(0)$ is also optimal for $P(T)$. $\overline{f}_P$ is averaged across members of each selected community, and subsequently averaged across the two selected communities. $\overline{K}_{MR}$ is similarly averaged, and then inverted to represent average affinity. Community function $\overline{P}(T)$ is averaged across the two selected communities. Black, cyan and gray curves are three independent simulations.

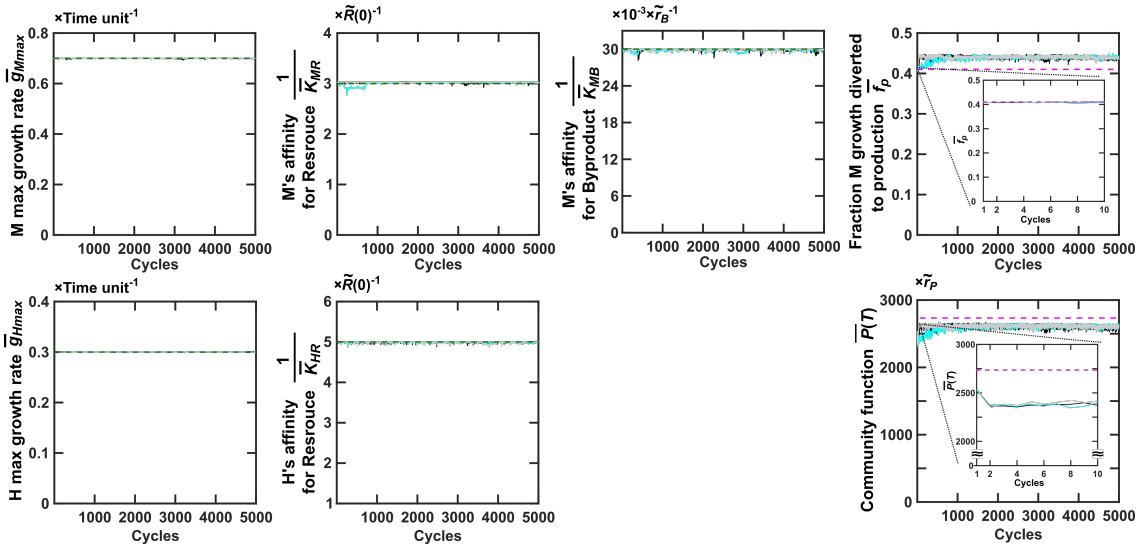

Figure S14: **Local optimality of community function $P^*(T)$.** We start each Newborn community with total biomass $N(0)$=100, all five growth parameters at their upper bounds, and $f_P^* = 0.41$ and $\phi_M^*(0) = 0.54$ to achieve $P^*(T)$. We then allow all five growth parameters and f_P to mutate while applying community selection. To ensure effective community selection (see the last section of Results), during community reproduction, we fix $N(0)$ to 100, and fix $\phi_M(0)$ to $\phi_M(T)$ of the previous cycle. We find that all five growth parameters remain at their respective evolutionary upper bounds. At the end of the first cycle (Cycle = 1 in insets), even though $\overline{f}_P$ has not changed, $\overline{P}(T)$ has already declined from the original magenta dashed line. This is because species interactions have driven $\phi_M(0)$ from the optimal $\phi_M^*(0)$ (=0.54) to near the steady state value (ϕ_M=0.73, compare with $\phi_{M,SS}$ represented by the green dashed line in Figure 1C bottom panel). Later, over hundreds of cycles, $\overline{f}_P$ gradually increases, which increases $\overline{P}(T)$. However, $\overline{P}(T)$ is still below maximal. This is because species composition gravitates toward steady state $\phi_{M,SS}$ which deviates from the optimal $\phi_M^*(0)$ ([54]). $\bar{g}_{Mmax}$, $\bar{g}_{Hmax}$, and $\overline{f}_P$ are obtained by averaging within each selected Adult community and then averaging across the two selected Adults. $K_{SpeciesMetabolite}$ are similarly averaged, and then inverted to represent average affinity. Green dashed lines: upper bounds of phenotypes; Magenta dashed lines: f_P^* and $P^*(T)$ when all five growth parameters are fixed at their upper bounds and $\phi_M(0) = \phi_M^*(0)$.

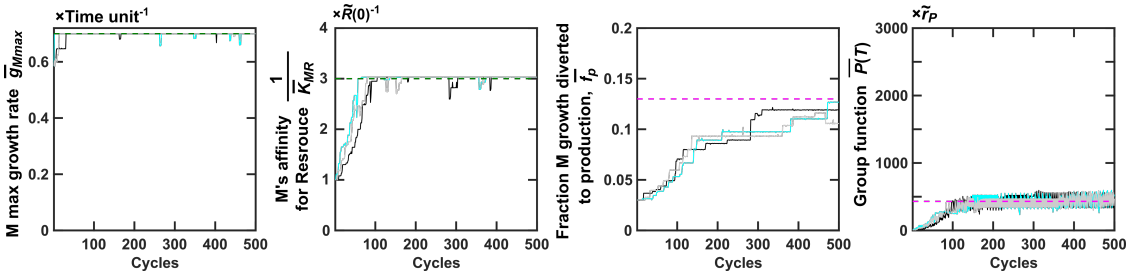

Figure S15: **Selection dynamics of M mono-species groups**. Phenotypes averaged over selected groups are plotted. Because Byproduct is in excess, K_{MB} terms are no longer relevant in equations (Figure S4, $R_M \ll B_M$). Upper bounds of g_{Mmax} and $1/K_{MR}$ are marked with green dashed lines. Magenta lines mark maximal f_P and $P(T)$ when g_{Mmax} and $1/K_{MR}$ are fixed at their upper bounds and when Byproduct is in excess.

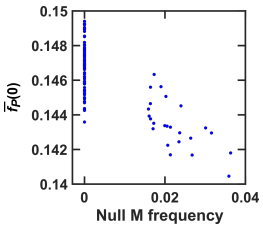

Figure S16: **The correlation between $\overline{f}_P(0)$ and the frequency of null M in a Newborn community.** As Newborns randomly sample M cells from the parent Adult community, their average $\overline{f}_P(0)$ partially correlates with the frequency of null M cells ($f_P = 0$).

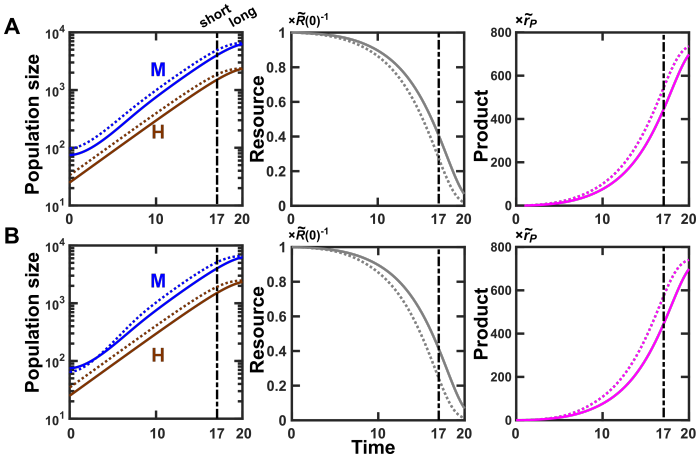

Figure S17: **Variations in community function can arise from non-heritable variations in Newborn compositions.** An average Newborn community (solid lines) has a total biomass of 100 with 75% M. (A) A "lucky" Newborn community (dotted lines), by stochastic fluctuations, has a total biomass of 130 with 75% M. Even though the two communities share identical $f_P = 0.1$, the Newborn with 130 total biomass has its M growing to a larger size (left), depleting more Resource (middle), and making more Product (right) by the end of short T (=17). (B) A "lucky" Newborn community (dotted lines), by stochastic fluctuations, has 100 total biomass with 65% M. Even though the two communities share identical $f_P = 0.1$, the Newborn with lower $\phi_M(0)$ (dotted) has its M enjoying a shorter growth lag and growing to a larger size (left), depleting more Resource (middle), and making more Product (right) by the end of short T (=17). In both cases, the difference between lucky (dotted) and average (solid) communities is diminished at longer T ($T = 20$) compared to shorter T ($T = 17$, dash dot line).

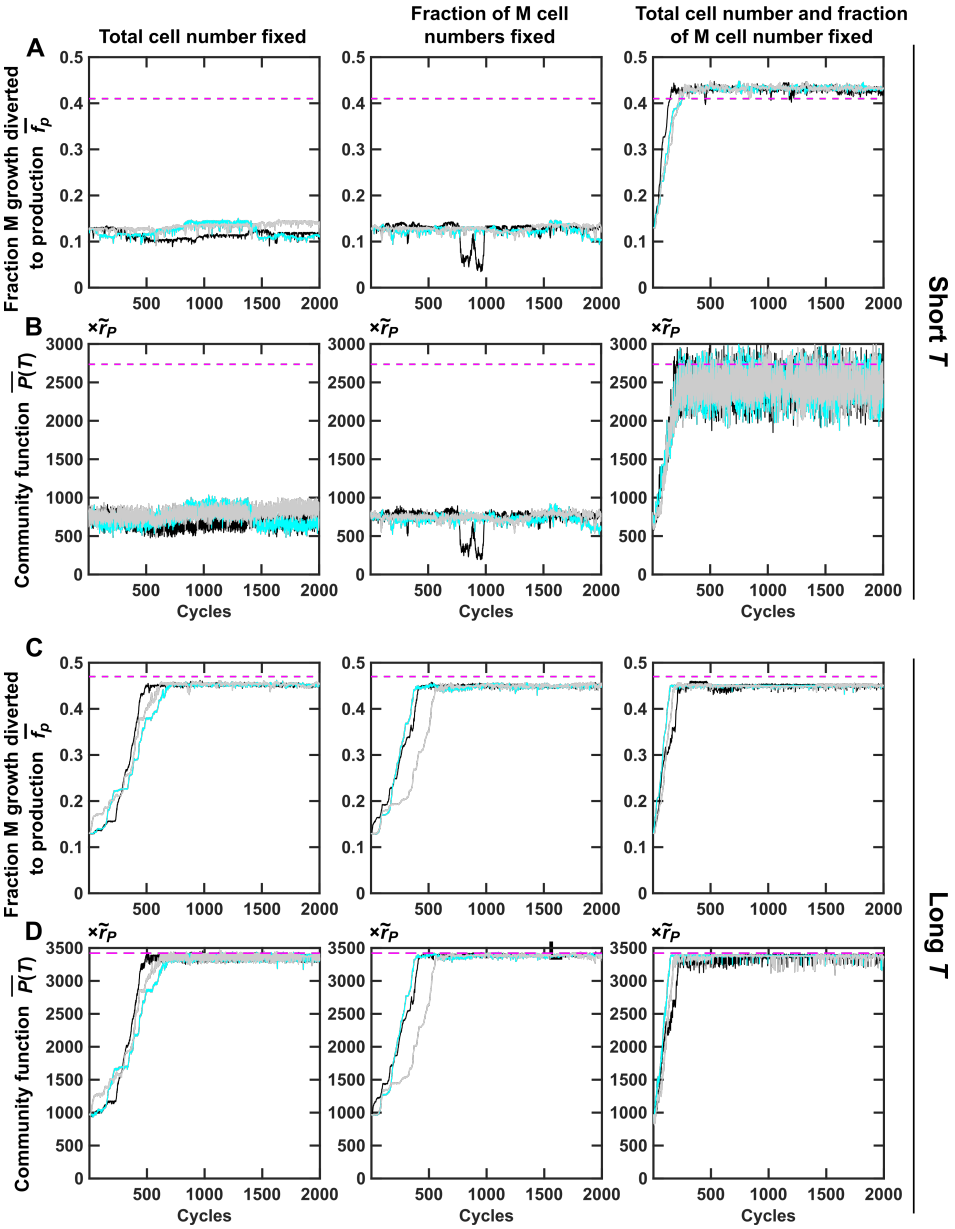

Figure S18: **Fixing H and M cell numbers (instead of biomass) during community reproduction allows short-T selection regimen to improve community function.** For left panels, the total cell number is fixed to $\lfloor N_0/1.5 \rfloor$ where $\lfloor x \rfloor$ means the largest integer without exceeding x. For center panels, the ratio between M and H cell numbers are fixed to $I_M(T)/I_H(T)$, where $I_M(T)$ and $I_H(T)$ are the number of M and H cells in the selected Adult community, respectively. For right panels, the total cell numbers are fixed to $\lfloor N_0/1.5 \rfloor$ and the ratio between M and H cell numbers are fixed to $I_M(T)/I_H(T)$. See Methods Section 6 for details of simulating community reproduction. Other legend details can be found in Figure 6.

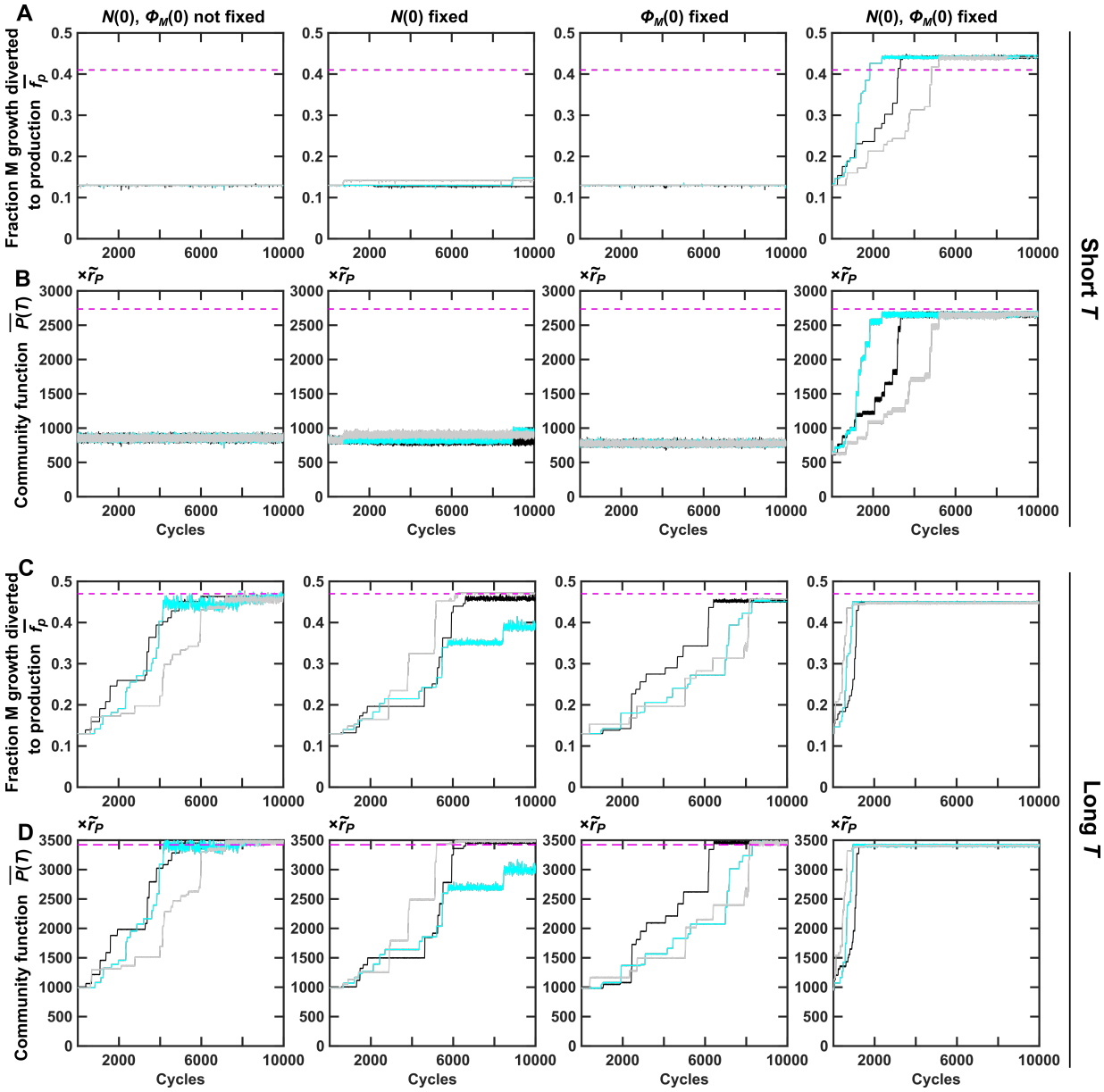

Figure S19: **Evolution dynamics of selected Adult communities at a mutation rate of 2×10^{-5} per cell per generation.** (**A, B**) At short maturation time ($T = 17$, Resource is not exhausted in an average community), fixing both $N(0)$ and $\phi_M(0)$ is required for community function to improve. (**C, D**) At long maturation time ($T = 20$, Resource is nearly exhausted in an average community), community function improves without needing to fix $N(0)$ or $\phi_M(0)$. When both are fixed, community function improves even faster. At this mutation rate, because the population size of a community never exceeds 10^4, a mutation occurs on average every 5 cycles, resulting in step-wise improvement in both $\overline{f}_P(T)$ and $\overline{P}(T)$. Other legend details can be found in Figure 6.

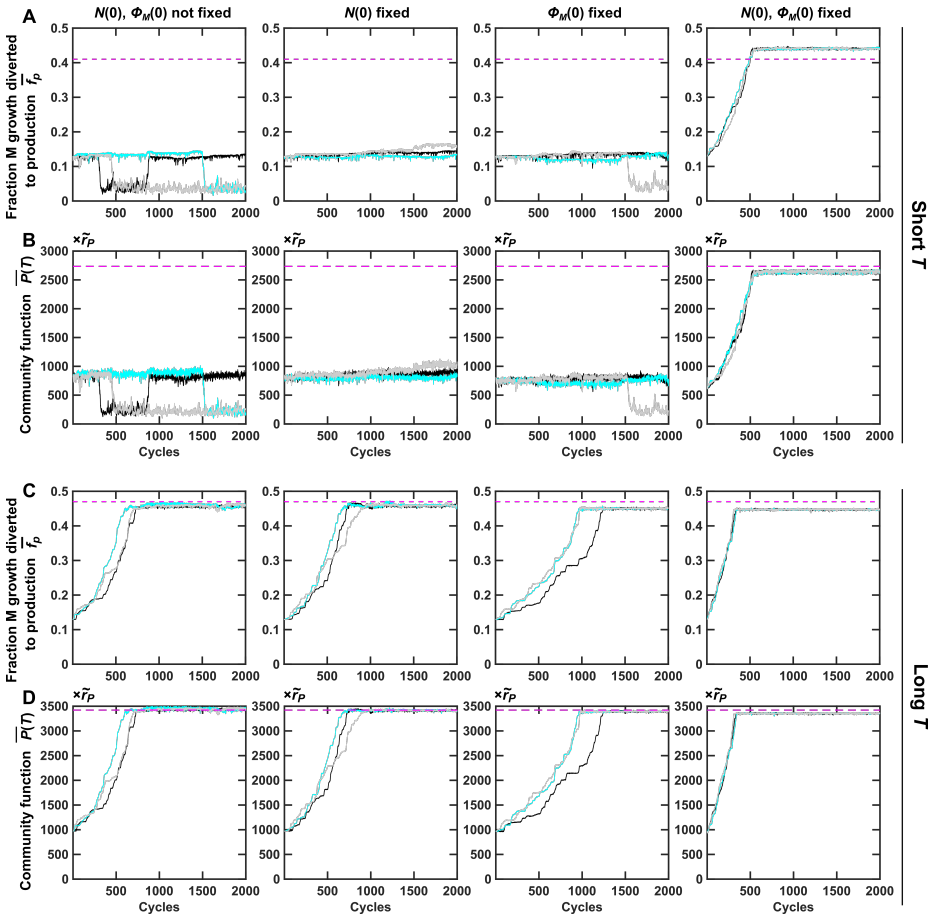

Figure S20: **Evolutionary dynamics of selected Adult communities under a different distribution of mutation effects.** Here, the distribution of mutation effects is specified by Eq. 15 where $s_+ = s_- = 0.02$ are constants. Other legend details can be found in Figure 6.

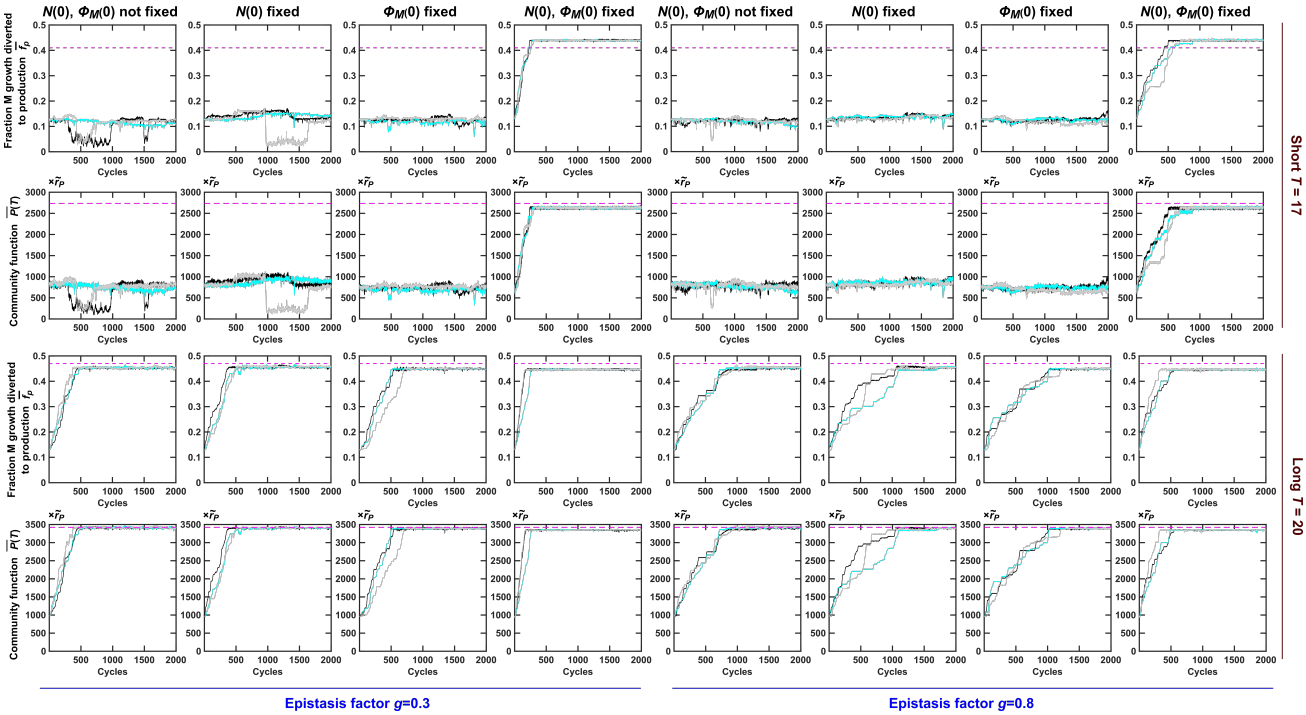

Figure S21: **Evolutionary dynamics of selected Adults when epistasis is considered.** When we incorporate different epistasis strengths (epistasis factor of 0.3 and 0.8), we obtain essentially the same conclusions as when epistasis is not considered (Figure 6). Other legend details can be found in Figure 6.

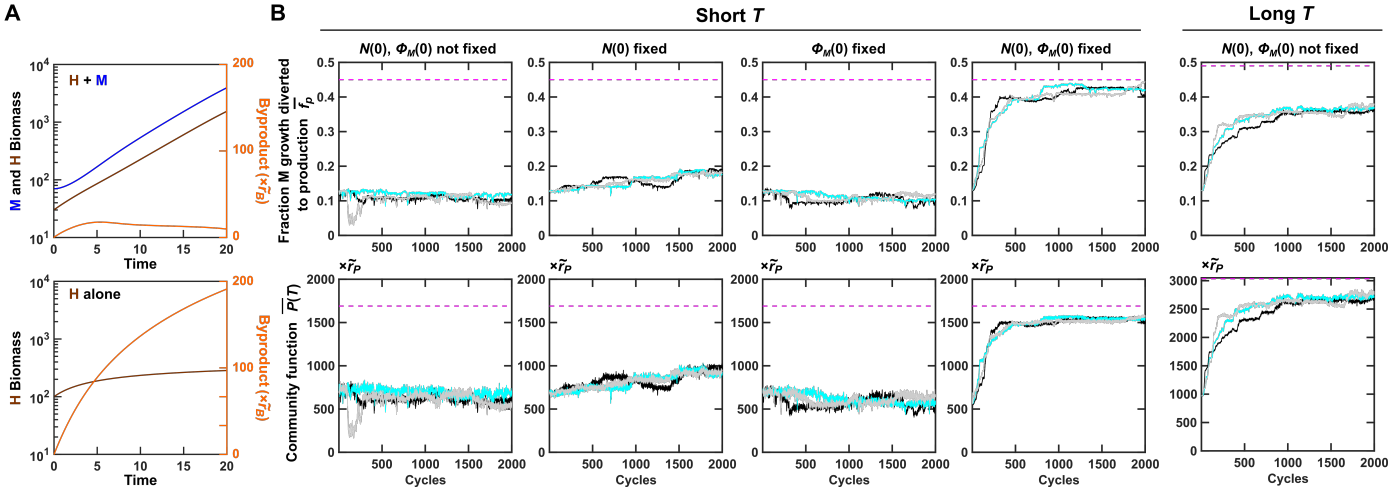

Figure S22: **Selection dynamics of mutualistic H-M communities.** In the mutualistic H-M community, H generates Byproduct which is essential for M but inhibitory to H. (**A**) H can grow to a high density in the presence of M (top) but not in the absence of M (bottom). (**B**) Similar to the commensal H-M community, selection works when non-heritable variations in $P(T)$ are suppressed either via fixing both $N(0)$ and $\phi_M(0)$ at short T (=17) or via extending T (=20). Other legend details can be found in Figure 6.

References

[1] Trevor D. Lawley, Simon Clare, Alan W. Walker, Mark D. Stares, Thomas R. Connor, Claire Raisen, David Goulding, Roland Rad, Fernanda Schreiber, Cordelia Brandt, Laura J. Deakin, Derek J. Pickard, Sylvia H. Duncan, Harry J. Flint, Taane G. Clark, Julian Parkhill, and Gordon Dougan. Targeted restoration of the intestinal microbiota with a simple, defined bacteriotherapy resolves relapsing Clostridium difficile disease in mice. *PLoS pathogens*, 8(10):e1002995, 2012.

[2] Souichiro Kato, Shin Haruta, Zong Jun Cui, Masaharu Ishii, and Yasuo Igarashi. Effective cellulose degradation by a mixed-culture system composed of a cellulolytic Clostridium and aerobic non-cellulolytic bacteria. *FEMS Microbiology Ecology*, 51(1):133–142, 2004.

[3] Stefanie Widder, Rosalind J. Allen, Thomas Pfeiffer, Thomas P. Curtis, Carsten Wiuf, William T. Sloan, Otto X. Cordero, Sam P. Brown, Babak Momeni, Wenying Shou, Helen Kettle, Harry J. Flint, Andreas F. Haas, Béatrice Laroche, Jan-Ulrich Kreft, Paul B. Rainey, Shiri Freilich, Stefan Schuster, Kim Milferstedt, Jan R. van der Meer, Tobias Groβkopf, Jef Huisman, Andrew Free, Cristian Picioreanu, Christopher Quince, Isaac Klapper, Simon Labarthe, Barth F. Smets, Harris Wang, Isaac Newton Institute Fellows, and Orkun S. Soyer. Challenges in microbial ecology: building predictive understanding of community function and dynamics. *The ISME Journal*, March 2016. 00001.

[4] Stephen R. Lindemann, Hans C. Bernstein, Hyun-Seob Song, Jim K. Fredrickson, Matthew W. Fields, Wenying Shou, David R. Johnson, and Alexander S. Beliaev. Engineering microbial consortia for controllable outputs. *The ISME Journal*, 10(9):2077–2084, September 2016.

[5] Jian Zhou, Qian Ma, Hong Yi, Lili Wang, Hao Song, and Ying-Jin Yuan. Metabolome profiling reveals metabolic cooperation between Bacillus megaterium and Ketogulonicigenium vulgare during induced swarm motility. *Applied and Environmental Microbiology*, 77(19):7023–7030, October 2011. 00038.

[6] R. E. Wheatley. The consequences of volatile organic compound mediated bacterial and fungal interactions. *Antonie van Leeuwenhoek*, 81(1-4):357–364, December 2002. 00123.

[7] Kwang-sun Kim, Soohyun Lee, and Choong-Min Ryu. Interspecific bacterial sensing through airborne signals modulates locomotion and drug resistance. *Nature Communications*, 4:1809, 2013.

[8] Matthew F Traxler, Jeramie D Watrous, Theodore Alexandrov, Pieter C Dorrestein, and Roberto Kolter. Interspecies interactions stimulate diversification of the Streptomyces coelicolor secreted metabolome. *mBio*, 4(4), 2013.

[9] Wenying Shou. Acknowledging selection at sub-organismal levels resolves controversy on pro-cooperation mechanisms. *eLife*, page e10106, December 2015.

[10] Hywel T. P. Williams and Timothy M. Lenton. Artificial selection of simulated microbial ecosystems. *Proceedings of the National Academy of Sciences*, 104(21):8918–8923, May 2007. 00036.

[11] William Swenson, David Sloan Wilson, and Roberta Elias. Artificial ecosystem selection. *Proceedings of the National Academy of Sciences*, 97:9110–9114, 2000.

[12] W. Swenson, J. Arendt, and D.S. Wilson. Artificial selection of microbial ecosystems for 3-chloroaniline biodegradation. *Environ Microbiol*, 2(5):564–71, October 2000.

[13] U. G. Mueller and J. L. Sachs. Engineering Microbiomes to Improve Plant and Animal Health. *Trends in Microbiology*, 23(10):606–617, October 2015.

[14] Ulrich G Mueller, Thomas Juenger, Melissa Kardish, Alexis Carlson, Kathleen Burns, Chad Smith, and David De Marais. Artificial microbiome-selection to engineer microbiomes that confer salt-tolerance to plants. *bioRxiv*, page 081521, 2016.

[15] Kevin Panke-Buisse, Angela C Poole, Julia K Goodrich, Ruth E Ley, and Jenny Kao-Kniffin. Selection on soil microbiomes reveals reproducible impacts on plant function. *The ISME journal*, 9(4):980, 2015.

[16] Jeremy J. Minty, Marc E. Singer, Scott A. Scholz, Chang-Hoon Bae, Jung-Ho Ahn, Clifton E. Foster, James C. Liao, and Xiaoxia Nina Lin. Design and characterization of synthetic fungal-bacterial consortia for direct production of isobutanol from cellulosic biomass. *Proceedings of the National Academy of Sciences*, 110(36):14592–14597, September 2013. 00024 PMID: 23959872.

[17] Kang Zhou, Kangjian Qiao, Steven Edgar, and Gregory Stephanopoulos. Distributing a metabolic pathway among a microbial consortium enhances production of natural products. *Nature biotechnology*, 2015.

[18] Hyun-Dong Shin, Shara McClendon, Trinh Vo, and Rachel R. Chen. Escherichia coli Binary Culture Engineered for Direct Fermentation of Hemicellulose to a Biofuel. *Applied and Environmental Microbiology*, 76(24):8150–8159, December 2010. 00000.

[19] Shen-Long Tsai, Garima Goyal, and Wilfred Chen. Surface Display of a Functional Minicellulosome by Intracellular Complementation Using a Synthetic Yeast Consortium and Its Application to Cellulose Hydrolysis and Ethanol Production. *Applied and Environmental Microbiology*, 76(22):7514–7520, November 2010.

[20] Babak Momeni, Kristen A Brileya, Matthew W Fields, and Wenying Shou. Strong inter-population cooperation leads to partner intermixing in microbial communities. *eLife*, 2:e00230, 2013. 00000.

[21] Sattar Taheri-Araghi, Serena Bradde, John T. Sauls, Norbert S. Hill, Petra Anne Levin, Johan Paulsson, Massimo Vergassola, and Suckjoon Jun. Cell-Size Control and Homeostasis in Bacteria. *Current Biology*, 25(3):385–391, February 2015.

[22] T Mankad and HR Bungay. Model for microbial growth with more than one limiting nutrient. *Journal of biotechnology*, 7(2):161–166, 1988.

[23] Richard E Lenski and Michael Travisano. Dynamics of adaptation and diversification: a 10,000-generation experiment with bacterial populations. *Proceedings of the National Academy of Sciences*, 91(15):6808–6814, 1994.

[24] Adam James Waite and Wenying Shou. Adaptation to a new environment allows cooperators to purge cheaters stochastically. *Proceedings of the National Academy of Sciences*, 109(47):19079–19086, 2012.

[25] Paul B Rainey and Katrina Rainey. Evolution of cooperation and conflict in experimental bacterial populations. *Nature*, 425(6953):72, 2003.

[26] Rafael U Ibarra, Jeremy S Edwards, and Bernhard O Palsson. Escherichia coli k-12 undergoes adaptive evolution to achieve in silico predicted optimal growth. *Nature*, 420(6912):186, 2002.

[27] Jeffrey E Barrick, Dong Su Yu, Sung Ho Yoon, Haeyoung Jeong, Tae Kwang Oh, Dominique Schneider, Richard E Lenski, and Jihyun F Kim. Genome evolution and adaptation in a long-term experiment with escherichia coli. *Nature*, 461(7268):1243, 2009.

[28] Toon Swings, Bram Van den Bergh, Sander Wuyts, Eline Oeyen, Karin Voordeckers, Kevin J Verstrepen, Maarten Fauvart, Natalie Verstraeten, and Jan Michiels. Adaptive tuning of mutation rates allows fast response to lethal stress in escherichia coli. *eLife*, 6(22939), 2017.

[29] Clifford Zeyl and J Arjan GM DeVisser. Estimates of the rate and distribution of fitness effects of spontaneous mutation in saccharomyces cerevisiae. *Genetics*, 157(1):53–61, 2001.

[30] Rafael Sanjuán, Andrés Moya, and Santiago F Elena. The distribution of fitness effects caused by single-nucleotide substitutions in an rna virus. *Proceedings of the National Academy of Sciences of the United States of America*, 101(22):8396–8401, 2004.

[31] Karen S Sarkisyan, Dmitry A Bolotin, Margarita V Meer, Dinara R Usmanova, Alexander S Mishin, George V Sharonov, Dmitry N Ivankov, Nina G Bozhanova, Mikhail S Baranov, Onuralp Soylemez, et al. Local fitness landscape of the green fluorescent protein. *Nature*, 533(7603):397–401, 2016.

[32] Dominika M Wloch, Krzysztof Szafraniec, Rhona H Borts, and Ryszard Korona. Direct estimate of the mutation rate and the distribution of fitness effects in the yeast saccharomyces cerevisiae. *Genetics*, 159(2):441–452, 2001.

[33] Celia Payen, Anna B Sunshine, Giang T Ong, Jamie L Pogachar, Wei Zhao, and Maitreya J Dunham. High-throughput identification of adaptive mutations in experimentally evolved yeast populations. *PLoS genetics*, 12(10):e1006339, 2016.

[34] George R. Price. Selection and Covariance. *Nature*, 227(5257):520–521, August 1970. 01240.

[35] John S Chuang, Olivier Rivoire, and Stanislas Leibler. Simpson's paradox in a synthetic microbial system. *Science (New York, N.Y.)*, 323(5911):272–275, January 2009.

[36] Adam James Waite, Caroline Cannistra, and Wenying Shou. Defectors Can Create Conditions That Rescue Cooperation. *PLoS Comput Biol*, 11(12):e1004645, December 2015. 00000.

[37] Kristina L Hillesland and David A Stahl. Rapid evolution of stability and productivity at the origin of a microbial mutualism. *Proceedings of the National Academy of Sciences*, 107(5):2124–2129, 2010.

[38] John L Spudich and Daniel E Koshland Jr. Non-genetic individuality: chance in the single cell. *Nature*, 262(5568):467, 1976.

[39] W. D. Hamilton. The genetical evolution of social behaviour I and II. *Journal of Theoretical Biology*, 7(1):1–52, July 1964.

[40] John Maynard Smith. Group Selection and Kin Selection. *Nature*, 201(4924):1145–1147, March 1964.

[41] Sewall Wright. Tempo and Mode in Evolution: A Critical Review. *Ecology*, 26(4):415–419, 1945.

[42] Michael J. Wade. A Critical Review of the Models of Group Selection. *The Quarterly Review of Biology*, 53(2):101–114, June 1978. ArticleType: research-article / Full publication date: Jun., 1978 / Copyright © 1978 The University of Chicago Press.

[43] William M Muir. Group selection for adaptation to multiple-hen cages: selection program and direct responses. *Poultry Science*, 75(4):447–458, 1996.

[44] David C. Queller and Joan E. Strassmann. Kin Selection and Social Insects. *BioScience*, 48(3):165–175, March 1998.

[45] Michael J Wade. An experimental study of kin selection. *Evolution*, pages 844–855, 1980.

[46] Arne Traulsen and Martin A. Nowak. Evolution of cooperation by multilevel selection. *Proceedings of the National Academy of Sciences*, 103(29):10952–10955, July 2006.

[47] L. Lehmann, L. Keller, S. West, and D. Roze. Group selection and kin selection: Two concepts but one process. *Proc Natl Acad Sci USA*, 104(16):6736–6739, April 2007.

[48] Benjamin Kerr. Theoretical and experimental approaches to the evolution of altruism and the levels of selection. *Experimental Evolution: Concepts, Methods, and Applications of Selection Experiments*, pages 585–630, 2009. 00006.

[49] Herwig Bachmann, Frank J Bruggeman, Douwe Molenaar, Filipe Branco dos Santos, and Bas Teusink. Public goods and metabolic strategies. *Current Opinion in Microbiology*, 31:109–115, June 2016. 00000.

[50] Katrin Hammerschmidt, Caroline J. Rose, Benjamin Kerr, and Paul B. Rainey. Life cycles, fitness decoupling and the evolution of multicellularity. *Nature*, 515(7525):75–79, November 2014.

[51] Martin A. Nowak. Five Rules for the Evolution of Cooperation. *Science*, 314(5805):1560–1563, December 2006.

[52] C. J. Goodnight and L. Stevens. Experimental studies of group selection: what do they tell us about group selection in nature? *The American Naturalist*, 150 Suppl 1:S59–79, July 1997.

[53] Herwig Bachmann, Martin Fischlechner, Iraes Rabbers, Nakul Barfa, Filipe Branco dos Santos, Douwe Molenaar, and Bas Teusink. Availability of public goods shapes the evolution of competing metabolic strategies. *Proceedings of the National Academy of Sciences of the United States of America*, 110(35):14302–14307, August 2013.

[54] Li Xie and Wenying Shou. Community function landscape and steady state species composition shape the eco-evolutionary dynamics of arti1cial community selection. *bioRxiv*, page 264697, 2018.

[55] Ronald Aylmer Fisher. *The genetical theory of natural selection: a complete variorum edition*. Oxford University Press, 1999.

[56] Nick Colegrave. Sex releases the speed limit on evolution. *Nature*, 420(6916):664–666, 2002.

[57] Philip J Gerrish and Richard E Lenski. The fate of competing beneficial mutations in an asexual population. *Genetica*, 102:127, 1998.

[58] Stephen T Chisholm, Gitta Coaker, Brad Day, and Brian J Staskawicz. Host-microbe interactions: shaping the evolution of the plant immune response. *Cell*, 124(4):803–814, 2006.

[59] Ruth E Ley, Micah Hamady, Catherine Lozupone, Peter J Turnbaugh, Rob Roy Ramey, J Stephen Bircher, Michael L Schlegel, Tammy A Tucker, Mark D Schrenzel, Rob Knight, et al. Evolution of mammals and their gut microbes. *Science*, 320(5883):1647–1651, 2008.

[60] Kevin R Foster, Jonas Schluter, Katharine Z Coyte, and Seth Rakoff-Nahoum. The evolution of the host microbiome as an ecosystem on a leash. *Nature*, 548(7665):43, 2017.

[61] Luc De Vuyst, Raf Callewaert, and Kurt Crabbé. Primary metabolite kinetics of bacteriocin biosynthesis by Lactobacillus amylovorus and evidence for stimulation of bacteriocin production under unfavourable growth conditions. *Microbiology*, 142(4):817–827, 1996.

[62] Babak Momeni, Kristen A Brileya, Matthew W Fields, and Wenying Shou. Strong inter-population cooperation leads to partner intermixing in microbial communities. *eLife*, 2, January 2013.

[63] Wenying Shou, Sri Ram, and Jose M. G. Vilar. Synthetic cooperation in engineered yeast populations. *Proceedings of the National Academy of Sciences of the United States of America*, 104(6):1877–1882, February 2007. 00137.

[64] Melanie JI Müller, Beverly I Neugeboren, David R Nelson, and Andrew W Murray. Genetic drift opposes mutualism during spatial population expansion. *Proceedings of the National Academy of Sciences*, 111(3):1037–1042, 2014.

[65] Thomas Egli. *Nutrition, microbial*. Oxford: Elsevier Academic Press, 2009.

[66] Kai Zhuang, Goutham N Vemuri, and Radhakrishnan Mahadevan. Economics of membrane occupancy and respiro-fermentation. *Molecular systems biology*, 7(1):500, 2011.

[67] Joan B Peris, Paulina Davis, José M Cuevas, Miguel R Nebot, and Rafael Sanjuán. Distribution of fitness effects caused by single-nucleotide substitutions in bacteriophage f1. *Genetics*, 185(2):603–609, 2010.

[68] Adrian WR Serohijos and Eugene I Shakhnovich. Merging molecular mechanism and evolution: theory and computation at the interface of biophysics and evolutionary population genetics. *Current opinion in structural biology*, 26:84–91, 2014.

[69] Adam Eyre-Walker and Peter D Keightley. The distribution of fitness effects of new mutations. *Nature reviews. Genetics*, 8(8):610, 2007.

[70] Michael A Stiffler, Doeke R Hekstra, and Rama Ranganathan. Evolvability as a function of purifying selection in tem-1 β-lactamase. *Cell*, 160(5):882–892, 2015.

[71] John W Drake. A constant rate of spontaneous mutation in dna-based microbes. *Proceedings of the National Academy of Sciences*, 88(16):7160–7164, 1991.

[72] Gregory I. Lang and Andrew W. Murray. Estimating the Per-Base-Pair Mutation Rate in the Yeast Saccharomyces cerevisiae. *Genetics*, 178(1):67–82, January 2008.

[73] Sasha F Levy, Jamie R Blundell, Sandeep Venkataram, Dmitri A Petrov, Daniel S Fisher, and Gavin Sherlock. Quantitative evolutionary dynamics using high-resolution lineage tracking. *Nature*, 519(7542):181, 2015.

[74] Lília Perfeito, Lisete Fernandes, Catarina Mota, and Isabel Gordo. Adaptive mutations in bacteria: high rate and small effects. *Science*, 317(5839):813–815, 2007.

[75] John H Gillespie. Molecular evolution over the mutational landscape. *Evolution*, 38(5):1116–1129, 1984.

[76] H Allen Orr. The distribution of fitness effects among beneficial mutations. *Genetics*, 163(4):1519–1526, 2003.

[77] Marianne Imhof and Christian Schlötterer. Fitness effects of advantageous mutations in evolving escherichia coli populations. *Proceedings of the National Academy of Sciences*, 98(3):1113–1117, 2001.

[78] Rees Kassen and Thomas Bataillon. Distribution of fitness effects among beneficial mutations before selection in experimental populations of bacteria. *Nature genetics*, 38(4):484, 2006.

[79] Darin R Rokyta, Paul Joyce, S Brian Caudle, and Holly A Wichman. An empirical test of the mutational landscape model of adaptation using a single-stranded dna virus. *Nature genetics*, 37(4):441, 2005.

[80] Darin R Rokyta, Craig J Beisel, Paul Joyce, Martin T Ferris, Christina L Burch, and Holly A Wichman. Beneficial fitness effects are not exponential for two viruses. *Journal of molecular evolution*, 67(4):368, 2008.

[81] Michael J Wiser, Noah Ribeck, and Richard E Lenski. Long-term dynamics of adaptation in asexual populations. *Science*, 342(6164):1364–1367, 2013.

[82] Lukasz Jasnos and Ryszard Korona. Epistatic buffering of fitness loss in yeast double deletion strains. *Nature genetics*, 39(4):550, 2007.

[83] Rafael Sanjuán, Andrés Moya, and Santiago F Elena. The contribution of epistasis to the architecture of fitness in an rna virus. *Proceedings of the National Academy of Sciences of the United States of America*, 101(43):15376–15379, 2004.

[84] Aisha I Khan, Duy M Dinh, Dominique Schneider, Richard E Lenski, and Tim F Cooper. Negative epistasis between beneficial mutations in an evolving bacterial population. *Science*, 332(6034):1193–1196, 2011.

[85] Santiago F Elena and Richard E Lenski. Test of synergistic interactions among deleterious mutations in bacteria. *Nature*, 390(6658):395, 1997.

[86] Carlos L Araya, Douglas M Fowler, Wentao Chen, Ike Muniez, Jeffery W Kelly, and Stanley Fields. A fundamental protein property, thermodynamic stability, revealed solely from large-scale measurements of protein function. *Proceedings of the National Academy of Sciences*, 109(42):16858–16863, 2012.

[87] Hsin-Hung Chou, Hsuan-Chao Chiu, Nigel F Delaney, Daniel Segrè, and Christopher J Marx. Diminishing returns epistasis among beneficial mutations decelerates adaptation. *Science*, 332(6034):1190–1192, 2011.

[88] Sergey Kryazhimskiy, Daniel P Rice, Elizabeth R Jerison, and Michael M Desai. Global epistasis makes adaptation predictable despite sequence-level stochasticity. *Science*, 344(6191):1519–1522, 2014.

[89] G. W. Luli and W. R. Strohl. Comparison of growth, acetate production, and acetate inhibition of Escherichia coli strains in batch and fed-batch fermentations. *Applied and Environmental Microbiology*, 56(4):1004–1011, April 1990.

[90] R C Lewontin. The Units of Selection. *Annual Review of Ecology and Systematics*, 1(1):1–18, 1970.

[91] A. Crameri, E. A. Whitehorn, E. Tate, and W. P. Stemmer. Improved green fluorescent protein by molecular evolution using DNA shuffling. *Nature Biotechnology*, 14(3):315–319, March 1996.

[92] Manfred T. Reetz and José Daniel Carballeira. Iterative saturation mutagenesis (ISM) for rapid directed evolution of functional enzymes. *Nature Protocols*, 2(4):891–903, April 2007.

[93] Eric T. Boder, Katarina S. Midelfort, and K. Dane Wittrup. Directed evolution of antibody fragments with monovalent femtomolar antigen-binding affinity. *Proceedings of the National Academy of Sciences*, 97(20):10701–10705, September 2000.

[94] Charles J Goodnight. The influence of environmental variation on group and individual selection in a cress. *Evolution*, 39(3):545–558, 1985.

[95] Melissa B Miller and Bonnie L Bassler. Quorum sensing in bacteria. *Annual Reviews in Microbiology*, 55(1):165–199, 2001.

[96] Clay Fuqua, Matthew R Parsek, and E Peter Greenberg. Regulation of gene expression by cell-to-cell communication: acyl-homoserine lactone quorum sensing. *Annual review of genetics*, 35(1):439–468, 2001.